Modeling Marine Systems

Volume I

Editor

Alan M. Davies
Principal Scientific Officer
Proudman Oceanographic Laboratory
Bidston Observatory
Birkenhead, Merseyside, England

CRC Press, Inc.
Boca Raton, Florida

Chapter 11

QUALITATIVE ASPECTS OF TOPOGRAPHIC WAVES IN CLOSED BASINS, GULFS, AND CHANNELS

Thomas F. Stocker and Kolumban Hutter

TABLE OF CONTENTS

I. ABSTRACT

After presenting the governing equation for topographic waves and discussing its properties and some known solutions in bounded and unbounded domains we point out an interesting and potentially useful connection between the spectrum of the topographic wave operator in a semi-infinite channel and that of the Schrödinger equation of an electron subject to the potential well. We then show that in closed basins there are three types of modal structures: global, basin-wide; small scale, basin-filled; localized. Effects of the variation of the topography on the dispersion relation are discussed and the influence of the curvature of an elongated basin on the dispersion relation and on the modal structure is studied. To further aid in the identification of the individual mode types in rectangular basins the current ellipses and the Stokes drift vectors are computed. A preliminary analysis of a double trench finally demonstrates how shelf waves may, through resonance, excite topographic waves in fjords or estuarine channels.

II. INTRODUCTION

Wave phenomena are among the distinctive features that can be observed in the velocity and temperature records of instruments which are moored in the ocean or in lakes. A large amount of them manifest themselves as barotropic or baroclinic gravity waves and, in enclosed basins, give rise to external or internal seiches with usually periods of a few hours and at most 1 to 2 d. Long periodic processes can, in general be attributed to the vorticity nature of the motion. Existence of these second-class waves is due to the rotation of the Earth and the variation of the bathymetry. In the ocean these so-called shelf waves have widely been identified as vorticity-dominated motions that are essentially trapped along the shores; in enclosed basins they form the topographic waves and enjoy a particularly rich structure. Their occurrence has been observationally corroborated in only a few individual cases (Lake Michigan, Lake Ontario, Lake of Lugano and Zurich, see Chapter 1 in Stocker and Hutter[1]), but the interpretation is partly controversial because of the scantiness of the data that were collected.

The aim of this study is to describe the structure of topographic waves in infinite and semi-infinite channels and in closed basins which in plan view form a rectangular region or a sector of an annulus and have a trough-like topography.

We first point out an interesting and potentially useful connection between the spectrum of the topographic wave operator in a semi-infinite channel and that of the Schrödinger equation subject to the potential well. It is then shown in detail that the topographic wave operator possesses a rich and dense spectrum with essentially three types of modal structures: global basin-wide modes, small-scale modes which fill the entire basin, and localized bay modes. Each of these modes has its distinctive structure; however, the modes cannot be ordered according to frequency, and often a mode with localized small-scale structure is hardly separated from another that "fills the entire basin". This aggravates identification of individual modes by observation. Dense nets of current meters and detailed analyses of time series that include rotary spectra and drift-current estimates may be necessary to arrive at reliable conclusions regarding mode identification. It is shown that drift currents of different modes are significantly distinct and may aid substantially in the interpretation of complicated data analyses. A preliminary analysis of a double trench finally demonstrates how shelf waves may excite topographic waves near river mouths or fjords. It also naturally indicates in which direction future research in topographic waves is likely to advance.

Consider the barotropic shallow-water equations subject to the rigid-lid assumption. Let ψ be the mass-transport stream function according to which

$$Hu = -\frac{\partial \psi}{\partial y}, \qquad Hv = \frac{\partial \psi}{\partial x} \tag{1}$$

$H(x,y) > 0$ is the water depth, and u,v are the vertically averaged velocity components in the x- and y- directions, respectively. The evolution equation for ψ evolves from the conservation law of potential vorticity and yields in general a first order hyperbolic partial differential equation that must be solved in the lake domain $\mathcal{D}$, subject to the boundary condition of no flow through the shore boundary $\partial\mathcal{D}$. Thus, the following boundary value problem emerges for ψ:

$$\begin{aligned} \tilde{\Pi}\psi &= 0, \qquad (x,y) \in \mathcal{D}, \\ \psi &= 0, \qquad (x,y) \in \partial\mathcal{D} \end{aligned} \tag{2}$$

Here $\tilde{\Pi}$ is the time-dependent wave operator

$$\begin{aligned} \tilde{\Pi} &= \frac{\partial}{\partial t} \nabla \cdot (H^{-1}\nabla(\cdot)) - \hat{z} \cdot \nabla(fH^{-1}) \times \nabla(\cdot) \\ &= \frac{\partial}{\partial t} E[\cdot] - J[fH^{-1},\cdot] \end{aligned} \tag{3}$$

in which f is the Coriolis parameter, $\hat{z}$ is a unit vector pointing in the direction opposite to the gravity vector, and ∇ is the horizontal gradient operator. Equation 3, when subject to f = constant, is called the *topographic wave operator*; it enjoys the following properties.[1]

- Whenever $J \equiv 0$, no waves can propagate. Any nonsteady solution is due to the presence of the rotation of the Earth and the variation of the bathymetric profile.
- The boundary value problem (Equation 2) is scale invariant, i.e., changing x,y by the scale [L] and the depth by the scale [H], leaves Equation 2 unchanged. This property is due to the rigid-lid assumption. Scrutiny indicates that it holds as long as [L] is small in comparison to the external Rossby radius

$$R = \frac{\sqrt{g[H]}}{f} \sim 500 \text{ km} \tag{4}$$

- Most significant, the topographic wave equation is invariant under conformal mappings. Indeed, in a general orthogonal curvilinear coordinate system $\xi = \xi(x,y)$, $\eta = \eta(x,y)$ the operators E and J read

$$\begin{aligned} E[\cdot] &= \frac{\partial}{\partial \xi}\left(\frac{J_2}{J_1}\frac{1}{H}\frac{\partial(\cdot)}{\partial \xi}\right) + \frac{\partial}{\partial \eta}\left(\frac{J_1}{J_2}\frac{1}{H}\frac{\partial(\cdot)}{\partial \eta}\right), \\ J[fH^{-1},\cdot] &= \frac{\partial}{\partial \xi}(fH^{-1})\frac{\partial(\cdot)}{\partial \eta} - \frac{\partial}{\partial \eta}(fH^{-1})\frac{\partial(\cdot)}{\partial \xi}, \end{aligned} \tag{5}$$

where J_1 and J_2 are the scale factors

$$J_1 = \left|\frac{\partial \xi}{\partial x}\right|, \qquad J_2 = \left|\frac{\partial \eta}{\partial y}\right|$$

Since under conformal mappings $J_1 = J_2$, Equation 5 reveals the stated invariance property. This property was pointed out and used by Johnson.[2,3] It was implicitly used also by Mysak.[4]

The invariance property of the topographic wave operator under conformal mappings is a useful tool, as a wealth of solutions can be generated from known solutions to special geometries. Thus Stocker and Hutter[1] have indicated, how shelf wave solutions along a hyperbolic shoreline can be obtained from Buchwald and Adams[5] shelf wave analysis for straight shorelines; and they show how straight-channel solutions can be used to construct topographic wave modes in hyperbolic channels. More important, Johnson[3] generates analytic topographic wave solutions in a semi-infinite channel by conformally mapping the infinite strip into a semi-infinite strip having a cut.

The conformal mapping *property* of the topographic wave operator has vastly enlarged the set of configurations for which topographic wave solutions are known, but the conformal mapping *technique* does not provide us with a tool to generate characteristically new solutions. A mode with a basin-wide structure in one domain will be stretched and torted in the transformed domain but it will still be basin wide. This is perhaps a limitation of its usefulness, as is the fact that bathymetric contour lines are transformed with the mapping so that topographies in the transformed domains may be very special and perhaps unrealistic.

Exact solutions to the boundary value problem (Equation 2) have been constructed in simple *bounded* and in special *infinite* domains. A summary of the existing solutions is given in Chapter 3 of Stocker and Hutter.[1] Lamb[6] is the first to present the topographic wave solution in a circular basin with parabolic bottom profile. Saylor, et al.[7] find exact formulas for modes in circular basins whose bottom profile varies radially according to a power law. Elliptical basins with parabolic bottom were treated by Ball,[8] and elliptical basins whose depth curves follow confocal ellipses are studied by Mysak,[4] Mysak et al.,[9] and Johnson.[2] All these solutions enjoy the property of having quantized real frequencies and wave numbers. Associated stream functions fill the entire basin and thus exhibit basin-wide structure. Figure 1 illustrates this for the three lowest modes in an elliptical lake with an exponential bottom profile.

The literature on topographic waves in unbounded domains is far more extensive, and it is impossible to do justice to all the relevant works. We thus limit our remarks to the essential properties and direct the reader to the reviews by Mysak[10] and Stocker and Hutter.[1,12] The configurations are generally domains that are infinitely long in the x-direction with one (shelf) or two (channel) shore boundaries parallel to it and with a topographic profile that varies only with y, the direction perpendicular to the x-direction. The following are characteristic properties of the solutions.[19]

- The spectrum, i.e., the dispersion relation is continuous: to each real frequency there is at least one real wave number. For a bounded slope parameter $S = |\partial H/\partial y|/H$ there is a countably infinite number of shelf modes and the dispersion relation is double valued, as shown in Figure 2 for exponential shelf waves.[5] Accordingly, long shelf waves are nondispersive, i.e., as $k \to 0$, $c_{gr} = \partial\sigma/\partial k = c = \sigma/k$. Phase and group velocities are the same. Moreover, for $0 < |k| < |k_0|$ the group velocity is positive, $c_{gr} > 0$, and energy and phase propagate in the same direction. For $|k| > k_0$, however, $c_{gr} < 0$ and the energy propagates against the phase. As $|k| \to \infty$ $\sigma \to 0$, $\sigma(k_0) = \sigma_0$ is called *critical frequency* or *cut-off frequency*.
- When S is unbounded at a point, $\sigma(k)$ is in general monotone with $\sigma \to \sigma_{max}$ as $k \to \infty$. The dispersion relation is now single valued.
- In doubly connected domains (topographic waves around islands) the above statements remain valid, but the spectrum is again quantized due to the 2π-periodicity of the x-coordinate.

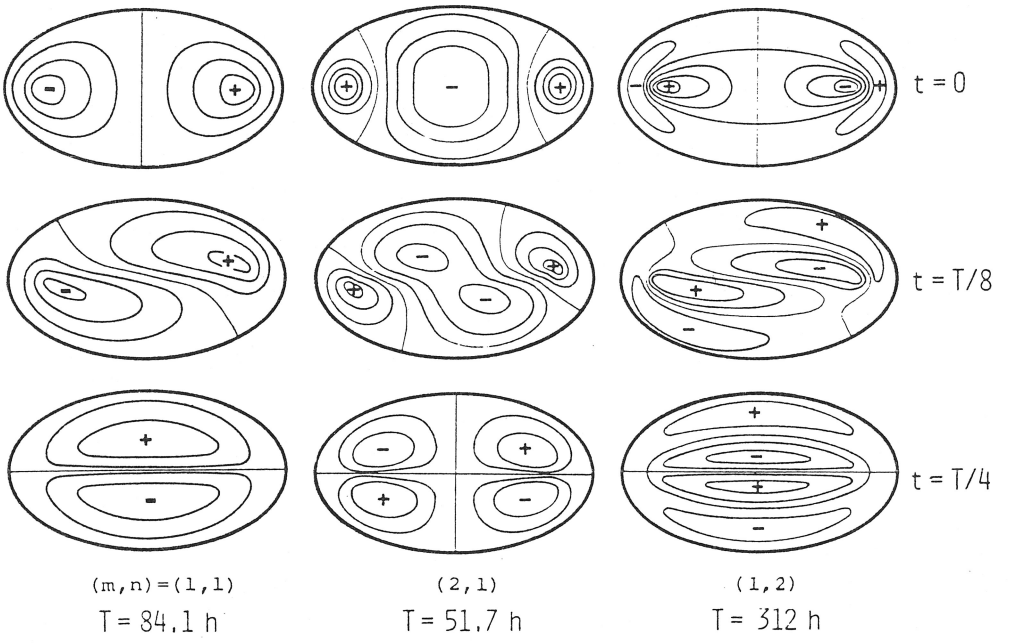

FIGURE 1. Stream line contours of the three lowest modes in an elliptical lake with exponential bottom. (From Johnson, E. R., *Geophys. Astrophys. Fluid Dyn.*, 37, 279, 1987. With permission.)

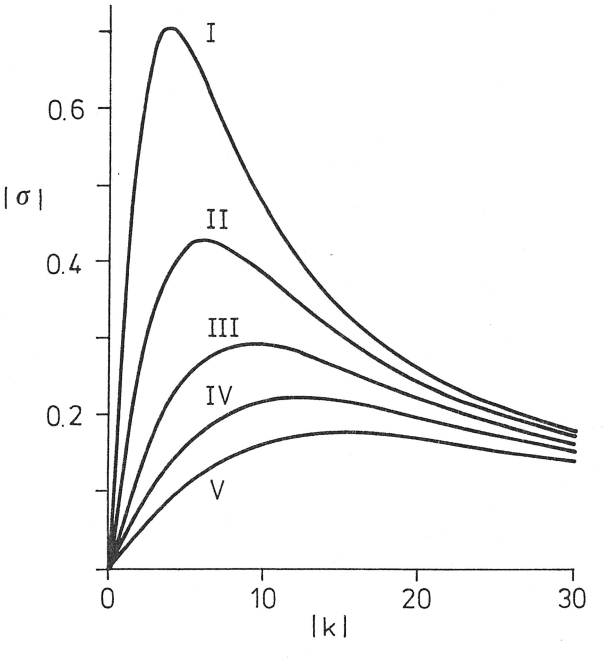

FIGURE 2. Dispersion relation σ(k) for the first five modes of the topographic wave equation on an exponential shelf with H (y) = ϵ exp (by), b = 5.4. (From Buchwald, V. T. and Adams, J. T., *Proc. R. Soc. London Ser. A*, 305, 235, 1968. With permission.)

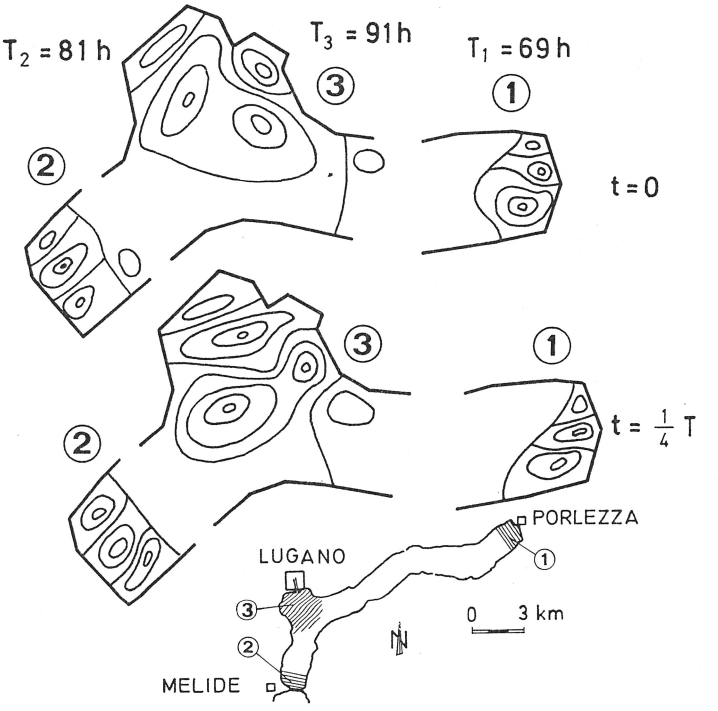

FIGURE 3. Three modes of long periodic waves in Lake of Lugano obtained by finite element technique. (From Stocker, T. and Hutter, K., *J. Fluid Mech.*, 185, 107, 1987. With permission.)

To our knowledge no analytical solutions of the boundary value problem (Equation 2) are known for domains and bathymetries H when non-separable equations emerge or equations cannot be transformed to special forms like in Ball's case of the ellipse with parabolic bottom. Neither have cases been studied where wave numbers would be complex. Such solutions are, however of significance as they would demonstrate existence of solutions of Equation 2 which show substantial wave activity in a relatively narrow region and die out as one moves away from these regions. The situation is not unlike that of Taylor reflections of Kelvin waves in a semi-infinite gulf.

Observations and, in particular, numerical computations for the Lake of Lugano indicate that such spatially evanescent solutions of the topographic wave equation do exist (see Figure 3). Trösch[13] found by using finite element techniques, that among other basin-wide modes, three independent bay modes, in the period range 69 to 91 h, existed with wave activity only in the bays shown in Figure 3. Existence of such modes can only be demonstrated if the *real branch* of the dispersion relation is extended to the *complex branch,* i.e., if complex wave numbers are also admitted.

In our semianalytical channel model[1,11,12] we have shown that dispersion relations *for each mode* are typically as shown in Figure 4. The real part of it (for $\sigma < \sigma_0$) is the typical shelf-wave-dispersion relation already shown in Figure 2. Above the cutoff frequency follows a complex domain, i.e., for $\sigma_0 < \sigma < \sigma_1$ to each σ there exist four complex wave numbers, two of which are conjugate complex. Above $\sigma = \sigma_1$ the wave number is purely imaginary. A complete system consists of a countably infinite number of such *mode units*. If σ is plotted against the modulus of k (for simplicity), then the dispersion relation for three modes is as shown in Figure 5. These special properties will be needed in the sequel.

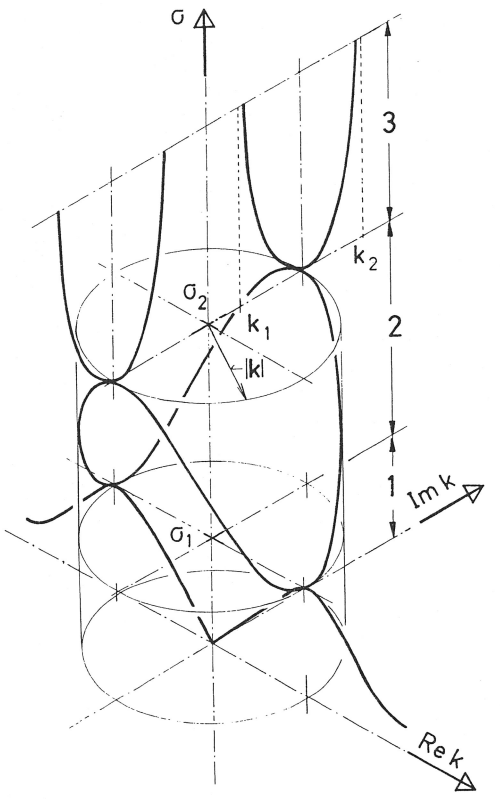

FIGURE 4. Schematic plot of the complex dispersion relation $\sigma(k)$ for an infinite channel. In regime 1, k is real; in regime 2, it is complex with the constant modulus $|k|$; and in regime 3, k is purely imaginary, taking asymptotic values k_1 and k_2 for large σ. (From Stocker, T. and Hutter, K., *J. Fluid Mech.*, 170, 435, 1986. With permission.)

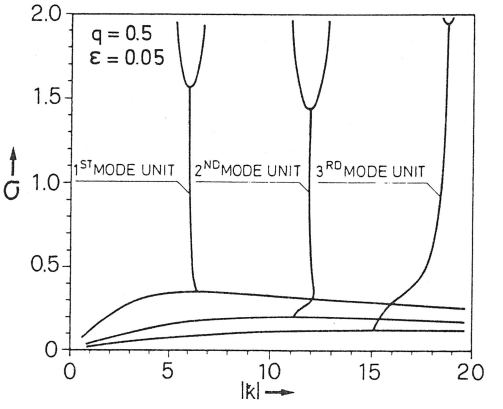

FIGURE 5. Modulus k of the third-order disperision relation for an infinite channel. (From Stocker, T. and Hutter, K., *J. Fluid Mech.*, 170, 435, 1986. With permission.)

III. BOUND STATES AND FREE STATES IN A GEOPHYSICAL SYSTEM

In this section a conspicuous correspondence is worked out between the structure of the solution space of the topographic wave equation and an other well-known and important problem in quantum physics. This correspondence helps to understand the problem of topographic waves in a more general framework and provides further important questions which remain to be answered in the future.

Topographic waves arise as periodic solutions of the linear, homogeneous boundary value problem (Equation 2). The operator (Equation 3) acts on the complex mass-transport stream function ψ, which must vanish on the boundary $\partial\mathcal{D}$ of the two-dimensional domain. Introduction of solutions proportional to $e^{-i\omega t}$, yields

$$\overline{\Pi} = -i\sigma\nabla \cdot H^{-1}\nabla - \hat{\mathbf{z}} \cdot \nabla H^{-1} \times \nabla \tag{6}$$

where the nondimensional frequency $\sigma \equiv \omega/f$ has been defined. Equation 6 can be written as

$$\Pi = -\Delta + \mathbf{V} \cdot \nabla \tag{7}$$

in which the vector function $\mathbf{V}$ is given by

$$\mathbf{V} = \nabla \log H - \frac{1}{i\sigma}\hat{\mathbf{z}} \times \nabla \log H \tag{8}$$

and contains the eigenvalue σ. Equation 8 gives the decomposition of the vector field $\underset{\sim}{V}$ into an irrotational and a solenoidal part.

An open domain $\mathcal{D}$ where the depth function H is smooth and satisfies the conditions

$$\begin{aligned} \frac{\partial H}{\partial x} &= 0, \qquad x_0 < x < \infty \\ |\nabla H|^2 &> 0, \qquad 0 < x < x_0 \end{aligned} \tag{9}$$

describes a semi-infinite channel in a (x,y)-coordinate system whose topography varies in both directions within the shore zone $0 < x < x_0$ and has a constant thalweg depth for $x > x_0$. By studying a semi-infinite channel that satisfies Equation 9, it was demonstrated in Stocker,[14,15] that the spectrum of Π is composed of a continuous and a discrete part. The two parts join at the critical frequency σ_0. Above this frequency, free topographic wave propagation for $x > x_0$ becomes impossible. However, for $\sigma > \sigma_0$ the spectrum is not empty; it is discrete, i.e., solutions of Equation 2 can be constructed provided the frequency takes the special values $\sigma = \sigma_i$ $(i = 1, 2, \ldots)$. Alternatively, in the interval $0 < \sigma < \sigma_0$ solutions with *any* frequency can be found. Figure 6 displays two typical modes belonging to the discrete and the continuous spectrum, respectively. Evidently, there is a distinct difference between these two representations.

Modes which belong to the discrete spectrum are *bound states* of the system. This is clear, because $\sigma > \sigma_0$ implies evanescent wave activity in the zone $x > x_0$ (see Figure 6). Although no wave energy is fed in from infinity, trapped wave energy can be found in the shore zone at *distinct* frequencies. Likewise, due to the existence of a cutoff frequency, energy cannot radiate away from the *open* shore zone. During one cycle vortices are formed close to the upper shore line. Their phase propagates in a right-bounded fashion along the

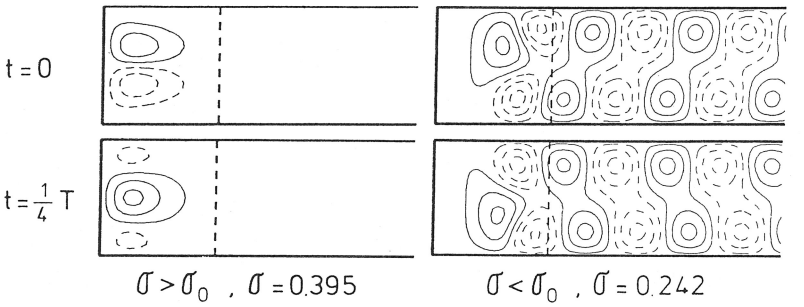

FIGURE 6. Solutions belonging to the discrete ($\sigma > \sigma_0$) and the continuous ($\sigma < \sigma_0$) spectrum. The discrete spectrum contains bound states: the stream function is spatially evanescent as one moves away from the bay zone, and the vortices remain trapped. Free states arise in the continuous spectrum: a wave incident from infinity is reflected in the bay. (From Stocker, T. and Hutter, K., *J. Fluid Mech.*, 185, 107, 1987. With permission.)

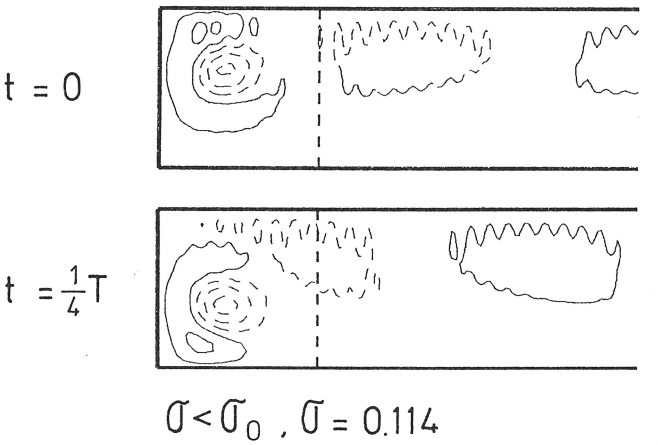

FIGURE 7. Resonance within the continuous spectrum. An incident wave excites a higher order bay mode.

channel endwall, where they evanesce at the opposite shore line. The continuous spectrum, on the other hand, shows *free states* of the system. Wave energy which is incident from infinity propagates along the upper boundary. The topography H which is acting like a repelling force in the shore zone $0 < x < x_0$ due to $\partial H/\partial x \neq 0$ induces a reflection of this energy flux and forces the vortices to follow the lines of constant f/H. It is this mechanism which produces the reflected wave of equal wave length which propagates towards infinity along the opposite channel shore. A characteristic quality of topographic waves is that to each frequency there always exists a short and a long wave (see Figure 4). Thus, wave energy could be distributed onto different modes. The study in Stocker[14,15] has shown, however, that for frequencies not close to σ_0 most of the reflected energy lies in the mode with the same wave number. Only close to σ_0 is the reflected energy contained in the mode with the second wave number. The continuous spectrum also contains *resonances*. These are bound states of higher transverse order. Since for the lowest order transverse mode periodic wave motion with $\sigma < \sigma_0$ is possible, trapped modes of higher order can be excited. A weak energy flux from infinity may then cause strong wave activity in the shore zone (Figure 7).

The above theoretical results still await verification in nature via carefully designed

mooring campaigns, or reinterpretation of measurements of long periodic signals which exhibited so far partly ambiguous portions. Nevertheless, the findings are of interest to both numerical and experimental oceanographers. They tell us that, in a numerical model of the ocean, not only tidal oscillations and propagating vorticity waves are to be expected when considering long periodic motion. Trapped vortex modes in large bays can also occur. We also point out that a separation of the motion due to gravity from that of vortex stretching (topographic waves) as is done in Equation 1 can not be achieved a priori under all circumstances. For a large basin or semi-open domain bay trapped modes with $\sigma > \sigma_0$ may well interact with gravity waves. This coupling was left undetermined by us.

Let us return to the conspicuous structure of the solution space of Equation 7 for a semi-infinite channel. This is a geophysical system which may allow trapped, free, and resonant solutions. For vorticity waves this fact was first demonstrated by Stocker and Hutter.[1] Other geophysical configurations have shown similar compound spectra: e.g., irrotational flow in a channel containing a cylindrical obstacle.[16] It must be emphasized, however, that our results are based on a semianalytic method. In Stocker and Johnson[17] the spectrum of the topographic wave operator is investigated for a simpler and more basic geometry of a semi-infinite channel. It is demonstrated that the number of both bay modes and resonances is governed by the bay topography. Further, estimates of the frequencies and the number of bay modes are deduced.

The topographic wave problem and its special solution space in the geophysical system of a semi-infinite channel enjoys a remarkable similarity with a well-known and thoroughly studied problem in modern physics. This correspondence is discussed here in order to provide a guide line for future theoretical and basic investigation concerned with the boundary value problem (Equation 2). The related problem is the stationary motion of an electron in the force field of a still proton. It can be understood by solving the Schrödinger Equation in space representation

$$\begin{aligned} \mathcal{H}\phi &= E\phi, \\ \mathcal{H} &= \Delta + V \end{aligned} \tag{10}$$

where $\mathcal{H}$ is the scaled Hamiltonian operator, V is a potential describing the attractive Coulomb force field of the still proton, E is the energy of the electron and ϕ is a complex probability function for the position of the electron. Ignoring the spherical geometry of the problem, one can study solutions in one single dimension x with a simple potential well of the form

$$\begin{aligned} V(x) &= \begin{cases} 0, & |x| > x_0, \\ -V, & |x| < x_0, \end{cases} \\ V &> 0 \end{aligned} \tag{11}$$

The structure of the solution, i.e., the probability of the particle position crucially depends on the eigenvalue E, the particle energy. Considering the potential (Equation 11), two cases must be distinguished.

For a particle with the energy E lower than the "well-energy" only bound states are allowed. This means that the electron is trapped within the potential well. Moreover, bound states are only possible for distinct energies $E = E_i$, $(i = 1, 2, \ldots)$. Consequently, for $E < 0$ there is a discrete spectrum containing solutions that are localized in the well. It is significant that both the values E_i and the number of possible trapped or bound states depend on the structure of the potential, i.e., on V and x_0.

Particles with arbitrary energy $E > 0$ can propagate outside the potential well. The classical theory predicts the complete transmission of a particle approaching the potential

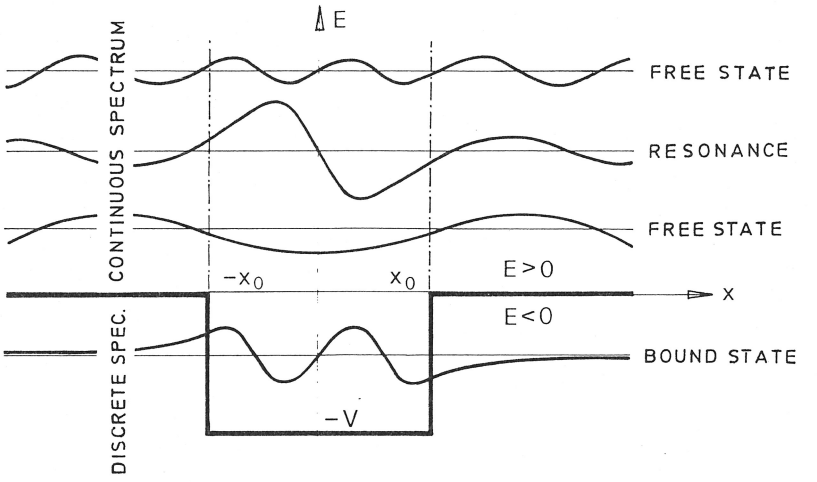

FIGURE 8. Model for an electron in the attractive force field (well potential) of a proton. For discrete $E < 0$ bound states prevail and the particles form a stable hydrogen atom. For $E > 0$ the electron is scattered by the proton; these are free states and occur for any $E > 0$. Resonances arise in the continuous spectrum.

well. Quantum theory, on the other hand, demonstrates that the particle is partly reflected and partly transmitted. At distinct energies the probability density within the potential well assumes a maximum. This is a resonant state where the residence time of the particle in the well is enlarged. Figure 8 summarizes these three qualitatively different solutions.

Comparing it with Figure 9, it is evident that the two solution spaces enjoy very similar properties. Both problems equally lead to three physically different states of the particle or of the topographic wave pattern. For large wave frequencies or negative particle energies only bound states are possible. Both particle and baymodes are not able to escape the well or the bay. In the opposite case when the frequencies do not exceed the critical cutoff, or the particle energies are positive, free states occur. Just as the particle is able to override the potential well and is not caught by it, the topographic wave impinging from infinity is reflected at the shore zone. Moreover, this reflection/transmission process depends on the frequency or energy of the wave or particle. For certain values the system exhibits a resonant state. This consists for the particle in an enlarged probability density to find it in the well. It amounts to a longer residence time of the free particle within the well. Equally, the water body in the open shore zone can be brought into resonance when a topographic wave with a certain frequency propagates towards the bay. Table 1 illustrates further formal correspondences of these two physically different problems. The remarkable correspondence of these two problems arises due to their similar mathematical description. This table therefore strongly suggests that the methods of mathematical physics which have been successfully applied to particle problems in quantum mechanics, could readily be employed for the topographic wave problem. There exists a vast literature on general principles of equations of the form Equation 10. These principles allow important estimates on the structure of the spectrum (e.g., is there a discrete part, etc.), on the behavior of solutions, on bounds for the eigenvalues, and many more. Further, criteria can be formulated which relate the structure of the spectrum to the coupling functions V or **V**. We encourage the mathematical oceanographer to tackle this challenging problem; the number of corresponding facts to a well-known problem may be promising.

We add some further speculations: the tunnel effect is an important mechanism in quantum physics. It predicts that a particle can "tunnel" through a potential barrier which his classical "brother" could never vanquish; an effect which was to experience a vast

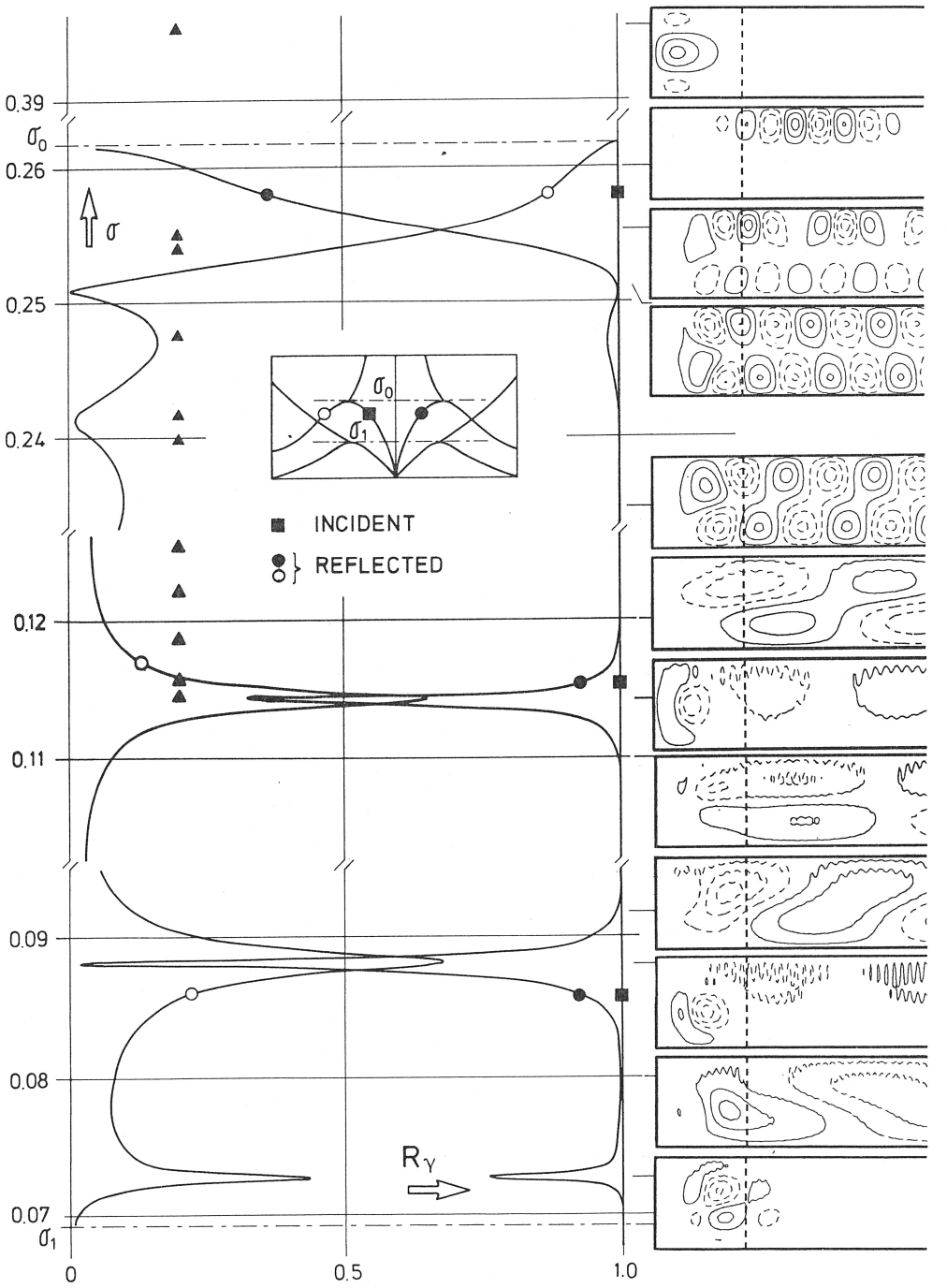

FIGURE 9. Spectrum of topographic waves in a semi-infinite channel consisting of a discrete ($\sigma > \sigma_0$) and a continuous part ($\sigma < \sigma_0$). Bound states exist in the discrete spectrum, free and resonant states occur in the continuous spectrum.[14,15]

technical and industrial application. Topographic wave energy likewise seems to exhibit the ability of tunneling[20]. For instance, imagine a continental shelf and an estuarine domain which is connected to the former. It remains to be verified, both theoretically and practically, that shelf wave energy could tunnel through an estuarine domain and excite at its end a resonant bay mode. Consideration of bathymetries which communicate with the open ocean

TABLE 1
Collection of Correspondences between a Well-Known Problem in Quantum Mechanics and Topographic Waves in a Semi-Infinite Channel with Equations 12 and 13

	Example in quantum mechanics	Topographic waves
Physical process described	Electron in an attractive Coulomb force field produced by a still proton	Topographic waves in an open domain of varying water depth
Equation considered	Schrödinger equation	Potential vorticity equation
Quantity	Probability density of particle location, scalar ϕ	Mass-transport stream function, scalar ψ
Differential operator	$\mathcal{H} \equiv -\Delta + (V - E)$	$\Pi \equiv -\Delta + \mathbf{V}(\sigma)\cdot\nabla$
Differential equation	$\mathcal{H}\,\phi = 0$	$\Pi\psi = 0$
Properties of equation	Partial, linear, second order, homogeneous	
Coupling to physical configuration	V, scalar potential of the Coulomb conservative force field	**V**, vector function of the gradient of the logarithmic depth field; **V** is not irrotational
Eigenvalue	E, particle energy	σ, wave frequency
Domain of integration	$\mathbb{R}^1$: $-\infty < r < \infty$ or $\mathbb{R}^3$: $0 < r < \infty$, $0 \le \varphi \le 2\pi$; $-\pi/2 < \theta < \pi/2$	$\mathbb{R}^2$: $0 < x < \infty$; $-B/2 \le y \le B/2$ Semi-infinite channel
Boundary conditions	ϕ finite or 0 for $\lvert r \rvert \to \infty$	ψ finite or 0 for $x \to \infty$ $\psi = 0$ for $x = 0$, $\lvert y \rvert = B/2$
Structure of spectrum	Spectrum consists of discrete and continuous part	
Discrete spectrum	For $E < 0$, countable set, finite or infinite number of eigenvalues dependent on V	For $\sigma > \sigma_0$, countable set? Number of eigenvalues? Dependence on **V**?
	$\phi \to 0$ for $\lvert r \rvert \to \infty$	$\psi \to 0$ for $x \to \infty$
	Bound states, electron, and proton form a stable hydrogen atom	Bound states, bay modes are trapped in the shore zone
Continuous spectrum	For $E > 0$,	For $0 < \sigma < \sigma_0$
	free states, electron is scattered by the proton	Free states, topographic wave is reflected in the shore zone
Resonances	For $E_i < 0$, $i = 1,2,\ldots$,	For $0 < \sigma_i < \sigma_0$; $i = 1,2,\ldots$
	Particle resides for a longer time close to the proton	Higher order bay mode is excited by incident wave

therefore must be viewed as being a *part* of a more complex water system. Interaction with oceanic vorticity wave motion should not be ignored a priori.

IV. GEOMETRY AND TOPOGRAPHY EFFECTS

In this section the influence of variation in topography and geometry of the basin is studied. It essentially is a summary of earlier work by Stocker and Hutter[1,11,12] and Stocker.[14,15]

A. VARIATION OF THE TOPOGRAPHY

Consider a semi-infinite channel with the transverse profile

$$h(x,y) = h_0(x)\left(1 + \epsilon - \left|\frac{2y}{B}\right|^q\right) \tag{12}$$

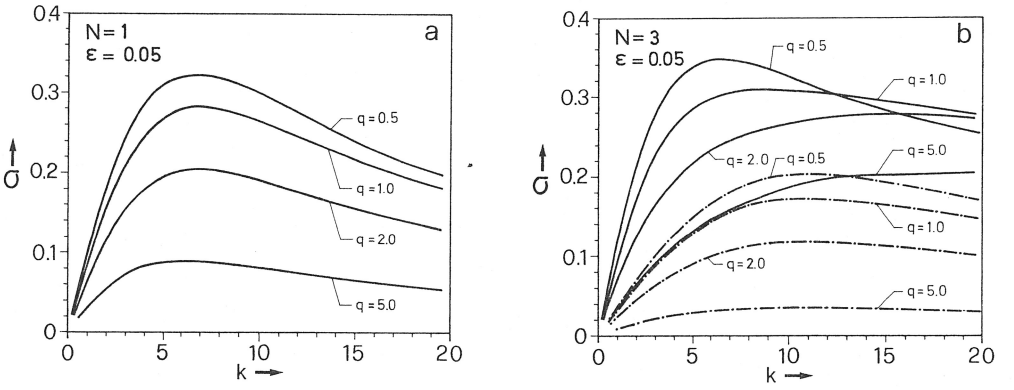

FIGURE 10. Effect of topography on the dispersion relation of the first mode (solid) and the second mode (dashed-dotted) in a channel. (a) N = 1, (b) N = 3. (From Stocker, T. and Hutter, K., *J. Fluid Mech.*, 170, 435, 1986. With permission.)

where $h_0(x)$ is the thalweg depth, ϵ a small sidewall parameter, B the channel width; $q < 1$ describes locally convex, $q > 1$ locally concave profiles. For $x > 0$ we define

$$h_0(x) = \begin{cases} \eta + \sin^p(\pi x/2x_0), & 0 < x < x_0, \quad p \geq 2, \\ \eta + 1 - \sin^{-p}(\pi(x_0 - x)/2x_0), & 0 < x < x_0, \quad p \leq -2, \\ \eta + 1, & x > x_0 \end{cases} \tag{13}$$

η is again a small shore depth parameter, p measures the "steepness" of the along-axis depth and x_0 determines the extent of the bay zone.

Numerical solutions of the topographic wave equation with the specifications of Equations 12 and 13 were constructed. Their frequencies depend quantitatively on the parameters introduced above. The value of the cutoff frequency for free wave propagation in $x > x_0$ depends only on the parameters q (and ϵ) which govern the global topography variations. They determine the exact form of the dispersion relation of which a parameter study of the real branches is shown in Figure 10 (a and b). Hence, q (and ϵ) determine the frequency range where free wave propagation in the far field is possible (namely for $\sigma < \sigma_0$). The q modifies also the transverse depth profile in the shore zone and therefore influences the frequencies of the bay modes. Figure 11 shows that this dependence is comparatively weak as values of σ only vary less than 10%.

The longitudinal depth variations can be modeled by the parameter p in Equation 13. It is clear that mostly modes confined to the shore zone, where the effect of p is experienced, will be affected by variation of p. Figure 12 gives the frequencies of the bay modes as functions of p. Whereas for $p < -2$ changes are moderate, they are significant for $p > 2$.

B. VARIATION OF THE GEOMETRY

The semi analytic method introduced by Stocker and Hutter,[1] permits a straightforward extension of the solution technique used for straight geometries to curved channels with constant curvature. This section closely follows Stocker.[14] Consider, therefore, basins whose plan view are sectors of annuli. The thalweg line is defined by the middle radius ($1/\kappa$). The assumption of constant κ and width B leads to a domain which has the shape of a ring. Consequently, the continuous dispersion relation would have to be subject to a periodicity condition. This quantization will not be imposed in the figures, simply because the full curve will provide a clearer understanding of the qualitative effects of curvature.

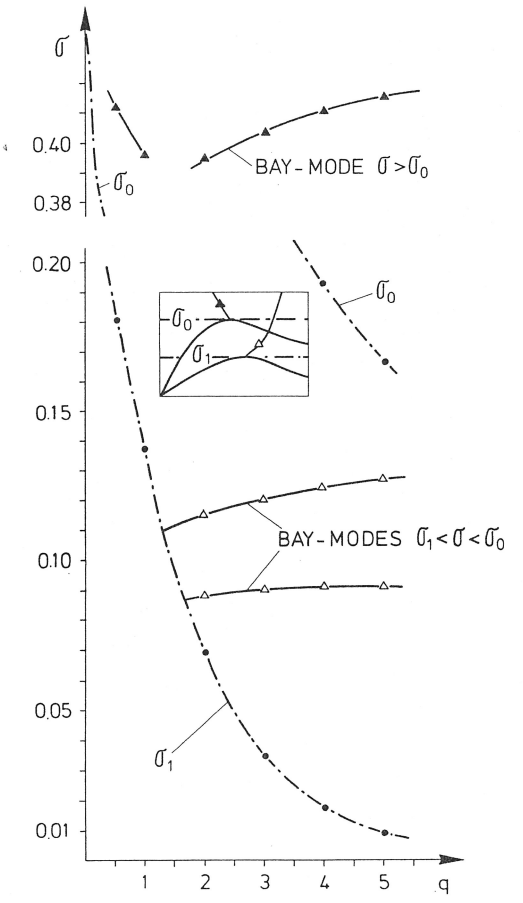

FIGURE 11. Frequencies of the resonances or bay modes in $\sigma_1 < \sigma < \sigma_0$ and a bay mode with $\sigma > \sigma_0$ as functions of the transverse topography parameter q; N = 2, ϵ = 0.05, p = 2, η = 0.01. The cutoff frequencies of the two mode units are indicated.[15]

Figure 13 shows the dispersion relation σ (k) of a third order model for the first two mode units. For $\kappa = 0$ the symmetry with respect to the vertical is visible, whereas for $\kappa > 0$ it is broken. For a given frequency all wave numbers are shifted to the right, which implies that curvature shortens waves for $k > 0$, whereas they become longer for $k < 0$. Recalling that the solutions are freely propagating waves (i.e., proportional to $e^{i(kx-\sigma t)}$), which are right bounded, it follows that the waves traveling along the inner (outer) shore line are longer (shorter) than in the case $\kappa = 0$. Further, the critical point (k_0^+, σ_0^+) in the domain $k > 0$ is translated to lower frequencies and larger wave numbers, and the opposite is true for (k_0^-, σ_0^-) in the domain $k < 0$. Consequently, there exists a frequency range $\sigma_0^+ < \sigma < \sigma_0^-$, where only waves with $k < 0$ can propagate. These are trapped along the inner shore line. If there existed eigenfrequencies in this range for a closed basin, their modal structure would exhibit a particular pattern with wave motion primarily at the inner shore line. This is discussed later. Table 2 lists the boundaries of these frequency ranges. For increasing curvature the values of σ_0^- and σ_0^+ lie farther and farther apart; this effect is weak for steep topographies. Note that from an observational point of view the difference is very small, e.g., $T_0^- \approx 57$ h and $T_0^+ = 63$ h for $q = 2$ and $\kappa = 0.2$, a difference that is unlikely to be detectable by field observations.

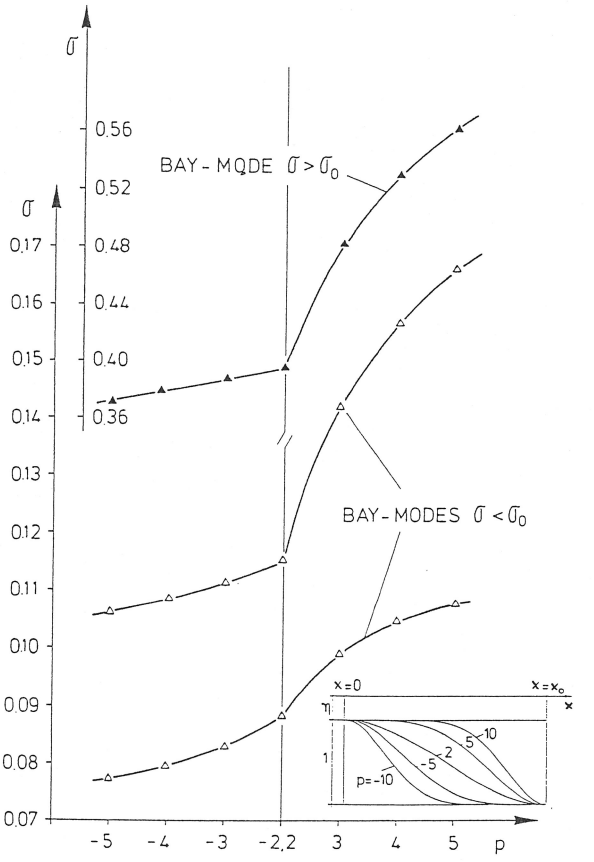

FIGURE 12. Frequencies of the resonances or bay modes in $\sigma_1 < \sigma < \sigma_0$ and a bay mode with $\sigma > \sigma_0$ as functions of the longitudinal topography parameter p; N = 2, q = 2, ϵ = 0.05, η = 0.01.[15]

On the other hand, for increasing κ and q the difference of the wave numbers increases. These properties are also displayed in Figure 14. Two mode units of the dispersion relation are given for different values of the topography and curvature parameters. The results support the findings listed in Tables 2 and 3.

So far we abstained from giving a physical explanation of the curvature effect and only listed and discussed the various alterations that arose in the dispersion relation because of the presence of curvature. In order to understand the physical mechanism which produces the asymmetry of $\sigma(k)$ we now work out the characteristic difference between the equations formulated in the natural coordinate system and in the Cartesian system. Topographic waves are described by the conservation of potential vorticity. This quantity contains three contributions: the curl of the velocity field representing the relative vorticity, the Earth's rotation as an additional vorticity, and the bottom topography. It is the relative vorticity which is primarily influenced by curvature. We give a rough analysis.

The potential vorticity Equation (2) in cylindrical coordinates (r, φ) describes topographic waves in a domain of constant curvature. Using Equation 5 and $J_1 = 1$, $J_2 = r$ for cylindrical coordinates implies

$$\frac{\partial}{\partial t}\left[\frac{1}{r}\frac{\partial}{\partial r}\left(\frac{r}{H}\frac{\partial \psi}{\partial r}\right) + \frac{1}{r}\frac{\partial}{\partial \varphi}\left(\frac{1}{rH}\frac{\partial \psi}{\partial \varphi}\right)\right] + \frac{\partial \psi}{\partial r}\cdot\frac{1}{r}\frac{\partial}{\partial \varphi}\left(\frac{1}{H}\right) - \frac{1}{r}\frac{\partial \psi}{\partial \varphi}\frac{\partial}{\partial r}\left(\frac{1}{H}\right) = 0 \quad (14)$$

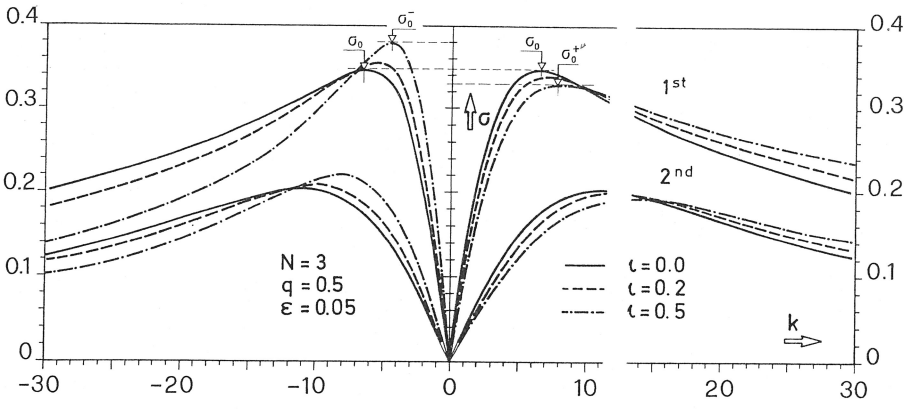

FIGURE 13. Dispersion relation of a third order model for various values of curvature. The parameters are N = 3, q = 0.5, ϵ = 0.05.[14]

TABLE 2
Frequencies $\sigma_0^{\pm}$ for $k \gtrless 0$ where $\partial\sigma/\partial k = 0$ for Different Values of Curvature κ and Topography q

q		$\kappa = 0$	$\kappa = 2.0$	$\kappa = 0.5$
	σ_0^-	0.2745	0.2799	0.2947
2.0	σ_0^+	0.2745	0.2708	0.2669
	$\Delta\sigma$	0	0.0091	0.0278
	σ_0^-	0.2081	0.2111	0.2188
5.0	σ_0^+	0.2081	0.2059	0.2033
	$\Delta\sigma$	0	0.0052	0.0155

Note: The parameters are N = 3, ϵ = 0.05, first mode unit.

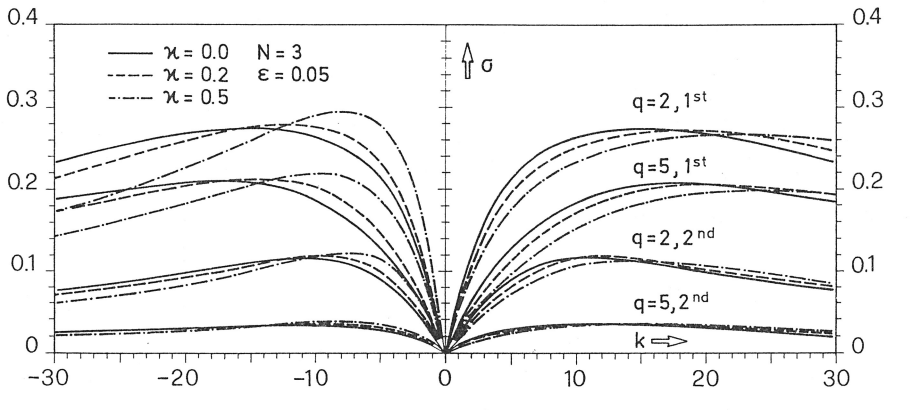

FIGURE 14. Curvature and topography effect on the dispersion relation.[14]

TABLE 3
Wave Numbers $k_0^{\pm}$ Corresponding to Table 2

q		κ = 0	κ = 0.2	κ = 0.5
	k_0^-	−14.9	−12.1	−7.83
2.0	k_0^+	14.9	17.8	21.9
	$k_0^+ - \lvert k_0^- \rvert$	0	5.7	14.1
	k_0^-	−17.7	−14.6	−9.83
5.0	k_0^+	17.7	20.7	25.1
	$k_0^+ - \lvert k_0^- \rvert$	0	6.1	15.3

Consider periodic solutions proportional to $e^{-i\sigma t}$ and domains where the depth profiles are azimuthally constant. Equation 14 then reduces to

$$\left[\psi_{rr} + \frac{1}{r^2}\psi_{\varphi\varphi} - \left(\frac{H_r}{H}\right)\psi_r + \frac{1}{r}\psi_r\right] + \frac{i}{\sigma}\left(\frac{H_r}{H}\right)\frac{1}{r}\psi_\varphi = 0 \tag{15}$$

In order to investigate the main effects of curvature on the wave properties it suffices to assume that the channel is only weakly curved. Such a domain has a radius of curvature $1/\kappa$, which is large compared with the channel width B. The arc length s is approximately given by

$$s = \frac{1}{\kappa}\varphi \qquad \frac{\partial}{\partial\varphi} = \frac{1}{\kappa}\frac{\partial}{\partial s} \tag{16}$$

whereby the varying position r was replaced by the constant radius of curvature $1/\kappa$. The same approximation is introduced in Equation 15 yielding

$$\left[\psi_{rr} + \psi_{ss} - \left(\frac{H_r}{H}\right)\psi_r + \kappa\psi_r\right] + \frac{i}{\sigma}\left(\frac{H_r}{H}\right)\psi_s = 0 \tag{17}$$

Equation 17 is the potential vorticity equation in Cartesian coordinates with the extra term $\kappa\psi_r$ incorporating to first order the effects of constant curvature.

The simple geometry of a weakly curved exponential trench with $1/\kappa \leq r \leq 1/\kappa + w$ allows the analytical solution of Equation 17. Let the water depth be given by

$$H(r) = e^{-2br}$$

and look for solutions

$$\psi = e^{iks} \cdot e^{-\left(b+\frac{\kappa}{2}\right)r} \cdot \sin\frac{n\pi\left(r - \frac{1}{\kappa}\right)}{B} \tag{18}$$

Inserting Equation 18 into 17 requires

$$\sigma = \frac{2bk}{k^2 + \left(b + \frac{\kappa}{2}\right)^2 + \left(\frac{n\kappa}{B}\right)^2} \tag{19}$$

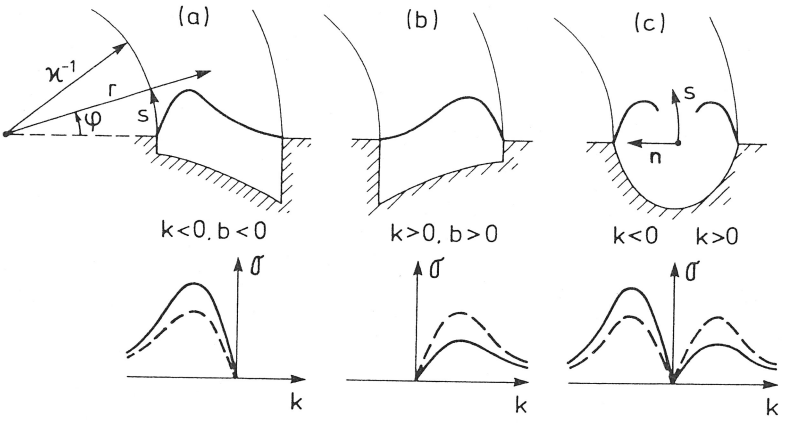

FIGURE 15. Two trench profiles (a) and (b) can model the effect of curvature in the natural coordinate system of a curved channel with parabolic bottom profile (c) by a "first order perturbation" of the TW-equation. The effects on the dispersion relations are indicated (dashed for $\kappa = 0$, solid for $\kappa \neq 0$) below.[14]

This is the dispersion relation of topographic waves in a bend. Figure 15 illustrates how the two curved trenches with $b < 0$, (Figure 15a) and with $b > 0$ (Figure 15b) can model the curved parabolic channel displayed in Figure 15c. On the northern hemisphere the phase of these waves propagates with the shallow water to its right. Hence, for $b < 0$ we must select $k < 0$ since $\sigma > 0$, and the wave travels along the inner curved shoreline at $r = 1/\kappa$. In this situation, $\kappa > 0$ generally increases frequencies, as can be inferred from Equation 19. A wave is trapped along the opposite outer shoreline if $b > 0$, i.e., the water is shallow towards $r = 1/\kappa + B$ and $k > 0$. Curvature $\kappa > 0$ then decreases frequencies.

The dispersion curves given below the two trenches explain the effect of curvature and are qualitatively in agreement with the behavior observed in Figures 13 and 14. The cutoff frequencies of waves traveling around convex bends are increased, whereas those of waves around concave bends are decreased. These fundamental alterations due to the introduction of curvature lead to an understanding of the modal structure of the eigenmodes in closed curved basins.

Figure 16 shows corresponding eigenmodes for different values of the curvature ordered according to frequency. Generally, curvature does not alter the eigenfrequency very much. Deviations of the eigenfrequencies for a strongly curved basin ($\kappa = 0.5$) from the values in the straight lake are throughout less than 5%. Eigenfrequencies decrease with increasing curvature. There is little hope to detect experimentally any effect of curvature on the eigenfrequency. The stream-function patterns, on the other hand, show more pronounced modifications.

The Ball-modes (basin wide, large scale) clearly demonstrate the influence of the shift of the wave numbers along either shore line. Although the total number of vortices remains constant when increasing κ, the number of gyres along the inner shore decreases in favor of that along the outer. Along with this, the inner vortices become larger.

As could be expected in advance, the stream function of the bay modes ($\sigma = 0.395$ and $\sigma = 0.115$) is hardly altered in the curved basin. This is rather obvious, because the bay does not "see" much of the curved basin. Mainly modes which consist of wave motion over the whole curved domain will be influenced by this change of geometry.

The channel modes (basin wide, small scale) demonstrate remarkable changes. By increasing the curvature, wave motion is significantly attenuated in the region towards the center of curvature. For $\kappa = 0.5$ (an extreme case) the eigenmode only consists of a trail of waves trapped to the outer shore line.

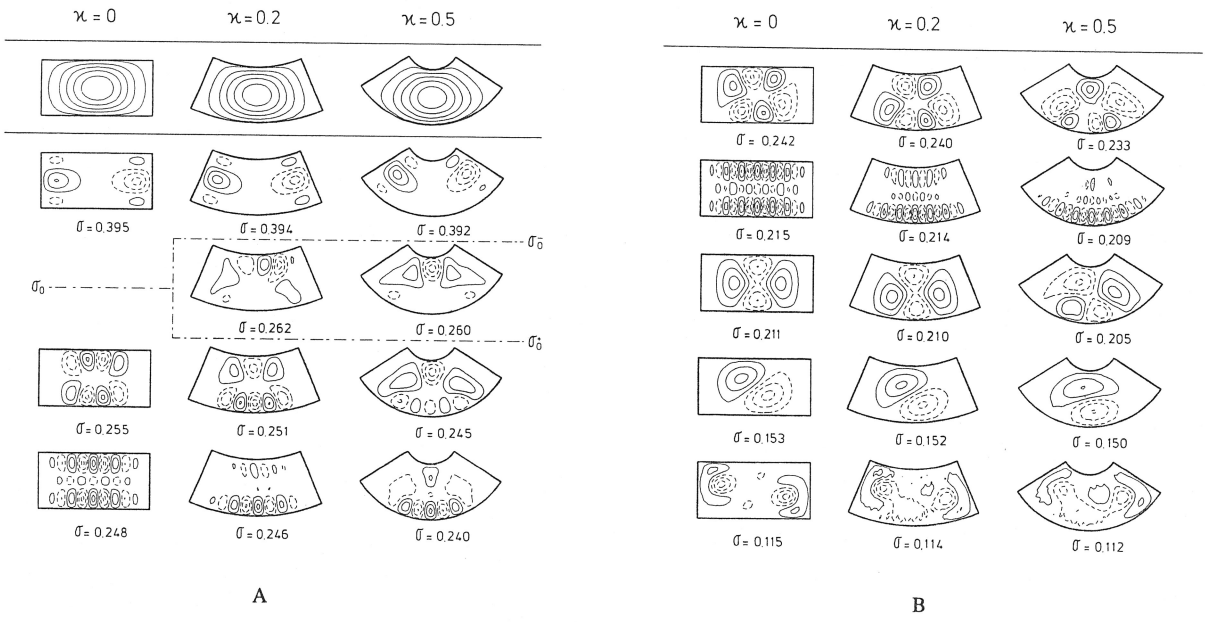

FIGURE 16. Comparison of eigenmodes in straight and curved basins; their lines of constant depth are shown in the top row. The modes are ordered for decreasing frequency. The cutoff frequency σ_0 splits in the case of curvature giving an interval $[\sigma_0^+, \sigma_0^-]$ in which the modes show unusual patterns.[14]

In the critical interval $I \equiv [\sigma_0^+, \sigma_0^-]$ there are indeed eigenfrequencies which exhibit the conjectured structure. Few large-scale vortices are trapped to the inner boundary of the basin. Solutions for $\kappa > 0$ with $\sigma \in I$ are structurally new. In the course of one cycle the vortices do not propagate around the basin but rather remain trapped in a domain close to the inner boundary. This mode, however is not a true bay mode since wave motion contains a contribution from the real wave number $k < 0$.

The above results suggest that with the exception of frequencies close to the cutoff, curvature effects can safely be ignored, since frequency shifts are small and most likely below the resolution of available instruments. On the other hand, Figure 16 indicates that detection of subtleties in the model structure would require a very high number of moored instruments in the transverse direction of the basin.

V. CURRENT FIELD

In this chapter the current structure in closed rectangular basins will be analyzed by constructing current ellipses and co-range and co-tidal lines and by evaluating drift currents for the three mode types. These quantities facilitate interpretation of the mode structures that are associated with detected frequencies via field observations.

A. CURRENT ELLIPSES AND TIDAL LINES

Consider the evolution of the transport vector $\hat{\mathbf{z}} \times \nabla\psi$ and of the velocity field $(\hat{\mathbf{z}} \times \nabla\psi)/H$ at fixed positions within the basin. An outstanding property of topographic waves is the fact that the field vector rotates either cyclonically or anticyclonically at a fixed position. Established statistical methods exist that permit calculation of the orientations of the rotation and of associated eigenfrequencies from periodograms of time series of velocity or transport field components. These rotary spectra are described in Gonella.[18]

In the present study all fields have harmonic time dependence, and, hence, the tip of a field vector will describe an ellipse. This ellipse is called transport ellipse (for the transport vector $\hat{\mathbf{z}} \times \nabla\psi$) or current ellipse (for the velocity vector $[\hat{\mathbf{z}} \times \nabla\psi)]/H$).

The qualitative structure of the stream function does not strongly depend on the values of the geometric and bathymetric parameters. It therefore suffices to examine one particular case. Figures 17 to 19 display eigenmodes of three examples of each type and their transport patterns. Some 63 positions within the rectangular basin are evaluated and the transport ellipse is plotted as a dashed (solid) curve if the transport vector rotates in the (counter) clockwise direction.

The first Ball-modes are characterized by a central area with counterclockwise rotation, (Figure 17). Its size depends on the mode, and we note that only the linear Ball-mode has a nonvanishing current vector in the center. This central area is surrounded by a region of clockwise and weak rotation. However, only Ball-modes with no "radial" node are given here; others emerge at much smaller frequencies, i.e., below the cutoff frequencies of the next mode units and would consist of more interlocking areas with different senses of rotation.

Figure 18 shows a selection of three bay modes. At the lake ends, wave activity is observed in the form of clockwise rotating currents. For higher bay modes these transport ellipses degenerate to nearly linear motion. It follows a zone of strong counterclockwise rotation, roughly at the position where the slope of the thalweg has a maximum. Beyond it, closer to the center, wave motion rapidly decreases and dies out.

The stream functions and transport ellipses of three channel modes are plotted in Figure 19. It is typical and could already be inferred from the stream-function plots, that there are bands along the long side of the basin. Close to the shoreline clockwise rotation is observed, being strongest in the middle of the elongated lake but weak at the long ends. Parallel to it follows a band where the current vectors rotate counterclockwise. Along the whole basin in the neighborhood of the thalweg line nearly no wave activity is experienced.

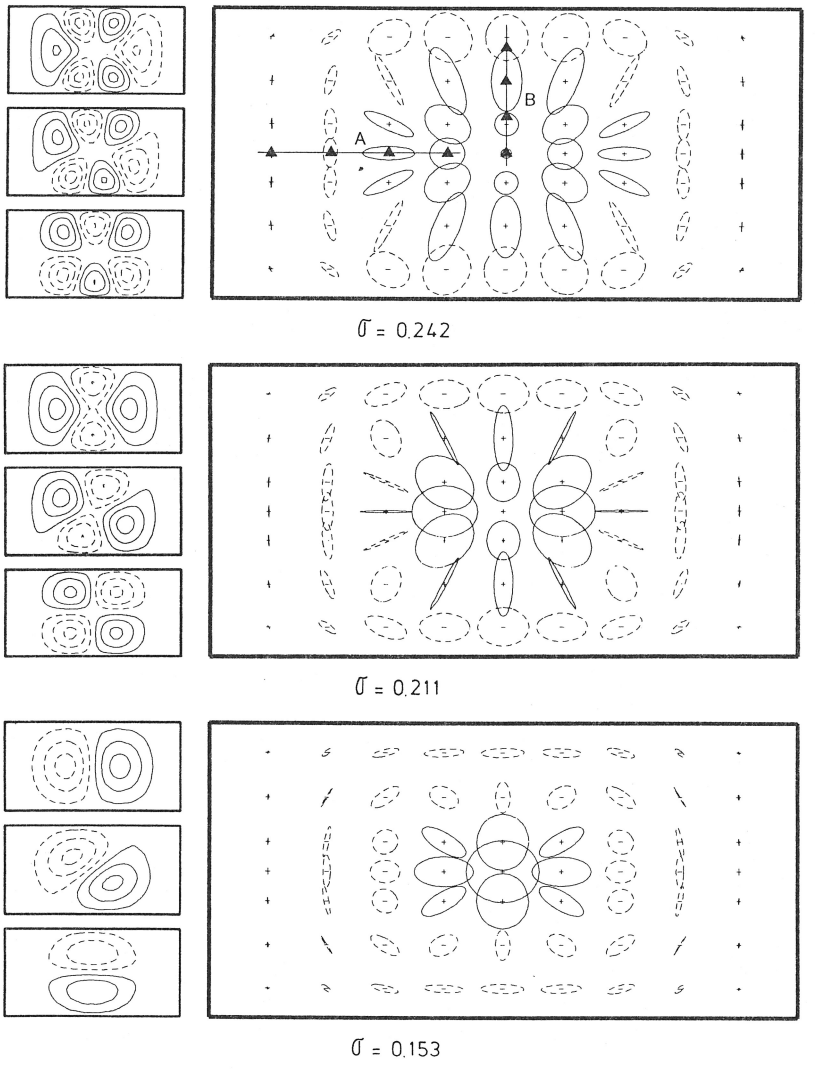

FIGURE 17. Stream function and transport ellipses for three Ball-modes. The small frames show contours of the stream function for t = 0 (bottom), t = T/8, t = T/4 (top). Transport ellipses are dashed (solid) for (counter) clockwise rotating transport vectors. ▲ indicate mooring sites on the linear arrays A and B, respectively.

The spatial and temporal interrelation between the fixed positions where individual mooring measurements can be taken must also be discussed. This can be readily achieved by calculating lines of constant phase and lines of constant amplitude of the transport stream function and the velocity vector fields.

Figures 20 to 22 display co-tidal and co-range lines of all important fields, i.e., the stream-function (scalar) and the transport field (in components). The linear Ball-mode (Figure 20) has the simplest structure. Co-range lines of the stream-function field are mainly circular, giving rise to a positive amphidromic point in the center of the lake. The co-tidal lines join at this point. The transport field (related to $\nabla\psi$) has now two amphidromies located at conjugate positions for both components; each exhibits a positive sense. Note that the transport field is weak towards the lake ends.

Figure 21 gives the quantities for the next higher Ball-mode (quadratic). The co-tidal

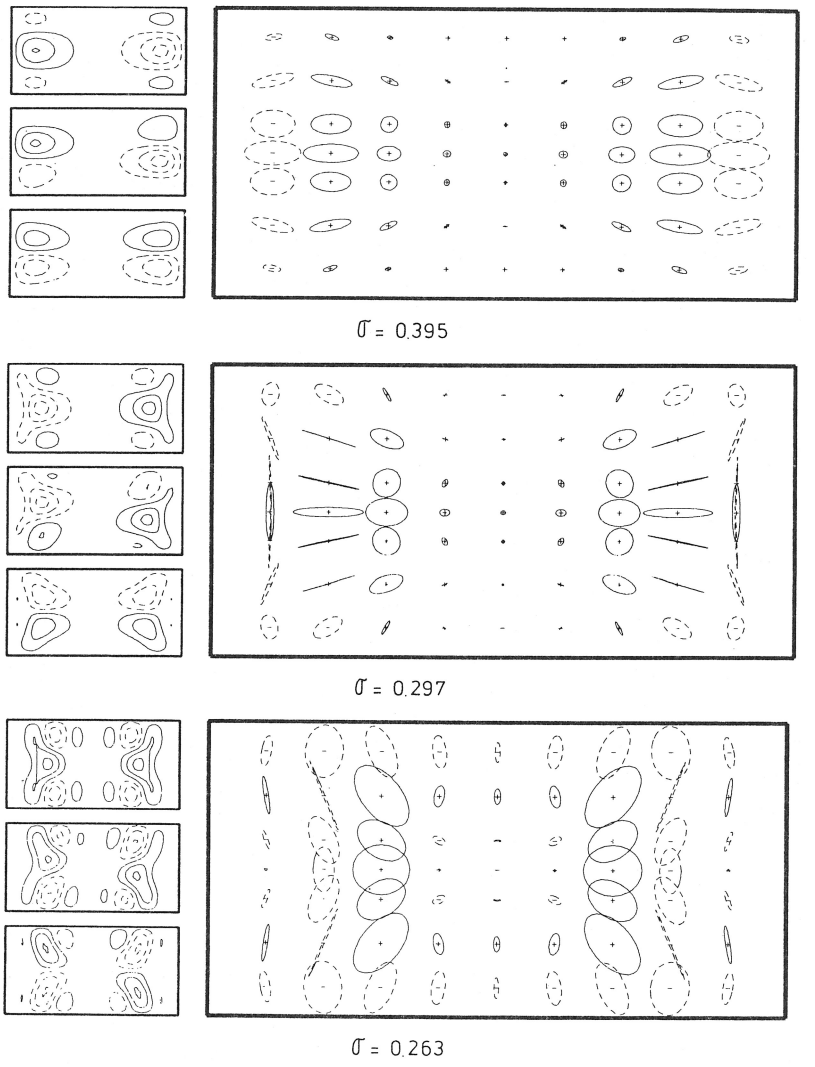

FIGURE 18. Same as Figure 17 for three bay modes.

lines repeat themselves once in the revolution, i.e., the co-tidal line pattern exhibits central symmetry. This was already evident from the stream-function pattern, as the phase does not complete an entire revolution around the basin during one cycle. The transport field shows now three amphidromic points for each component, all of which are positive.

The patterns of a bay mode are different, (Figure 22). Co-phase lines are mainly straight, joining at one or two positive amphidromic points at the center of the basin. The v-component of the transport has a nodal line across the basin near the lake end. In view of the smaller spatial scale of the vortices the channel modes (not shown here) have much more complicated patterns.

B. PARTICLE PATHS

A consistent linear wave theory predicts closed particle paths. Within this linear approximation, the path line represents the scaled trace of the tip of the Eulerian velocity vector, the current ellipse. Figures 17 to 19 give an impression of the shape and orientation of these particle paths. Note, however, that they apply for transport ellipses and therefore depth-integrated path lines.

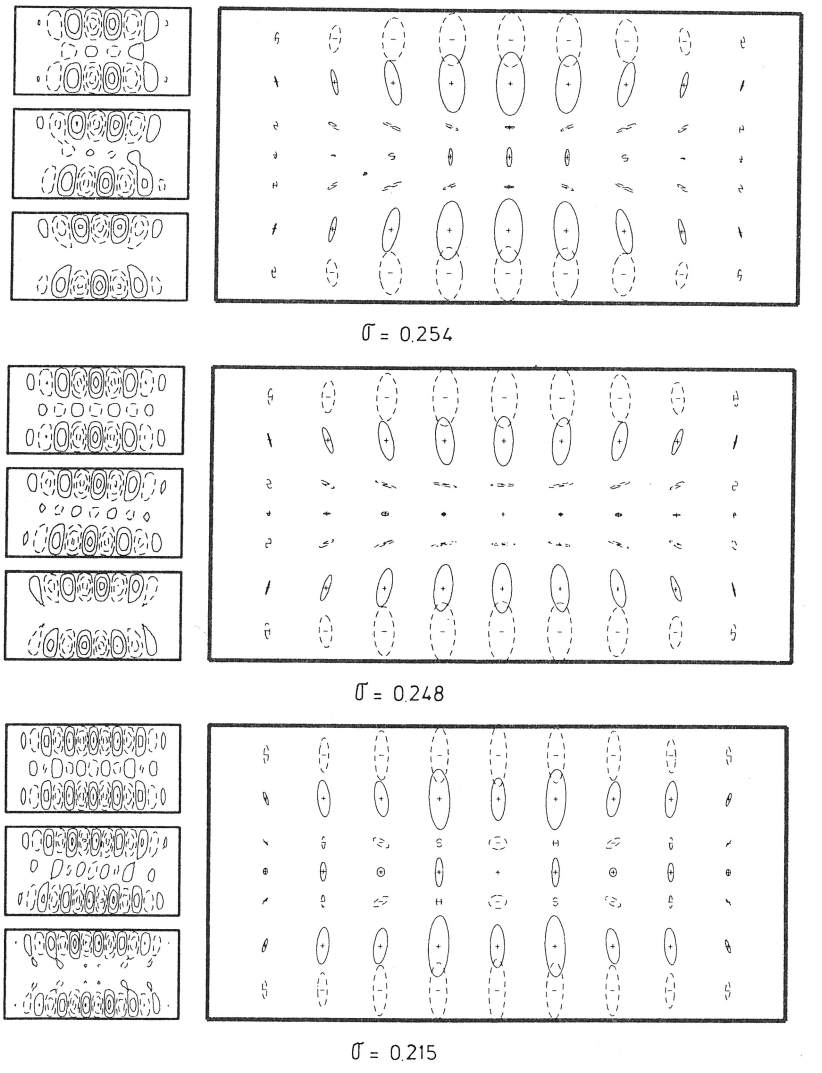

FIGURE 19. Same as Figure 17 for three channel modes.

The linear theory can be extended to provide a first estimate of the particle path caused by advection; this nonlinear effect, called Stokes drift, causes a net displacement during one cycle due to the spatial variation of the velocity field. Observationally, the Stokes drift manifests itself as a mean transport.

Figures 23 to 25 show the depth-integrated Stokes drift and correspond to Figures 17 to 19. It is a property of the Ball-modes (Figure 23) that the counterclockwise propagating gyres produce a net drift in the clockwise direction. This induced circulation is closer to the boundaries the higher the Ball-modes are. For the quadratic and the higher Ball-mode a weak cyclonic rotation in the lake center is observed. At the lake ends there is no drift.

The bay modes in Figure 24 exhibit significant transport at the lake ends, each in a different fashion. The mode with $\sigma = 0.395$ has a pronounced drift along the short sides of the basin against the direction of phase propagation. The lower left and top right corners act as sources; the others are sinks of the drift current. The next bay mode shows a pair of lateral gyres and the structure of the stream function of the mode with $\sigma = 0.263$ implies a drift along the ends of the long sides. The role of the sources and sinks is now interchanged.

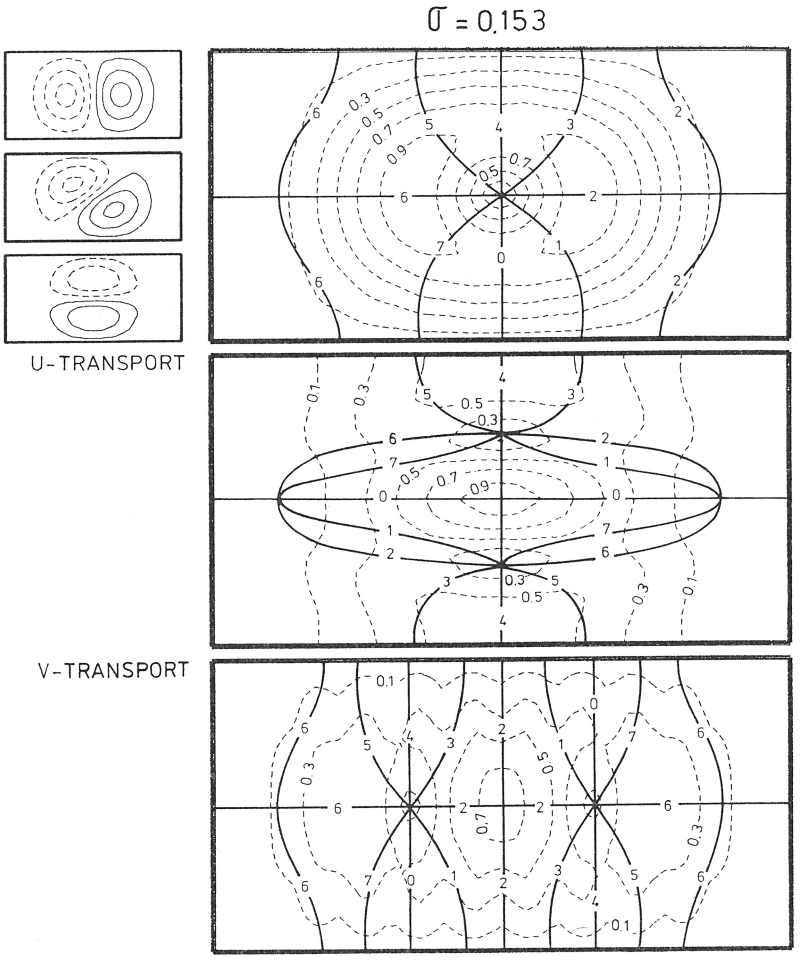

FIGURE 20. Lines of constant phase (solid; co-tidal lines) and lines of constant amplitude (dashed; co-range lines) of the stream function, the u-component (along thalweg axis) of the transport and the v-component for the linear Ball-mode. The numbers labeling lines of constant phase correspond to multiples of an eighth of a period; those of constant amplitude indicate the fraction of the maximum amplitude.[14]

Figure 25, finally, shows drift vectors for the channel modes. They hardly differ from each other, and the pattern consists of two near-shore drifts in opposite direction to phase propagation. The drift is experienced only close to the long sides of the basin and most of the lake has no transport at all. Opposite corners again act as sources and sinks, respectively. The Stokes drift has a particular sense of direction which is mainly clockwise around the basin (on the northern hemisphere). Nevertheless, the three mode types have different transport properties: Ball-type modes exhibit a circular pattern confined to the center of the lake. Bay and channel-type modes show a straight drift current along the short and long sides of the basin, respectively. This again underlines that knowledge of the modal type is of particular importance.

VI. THE DOUBLE TRENCH

In this section a crude model is presented which shall give an idea of the behavior of shelf waves near river mouths, fjords, or estuarine domains. The simplicity of the model,

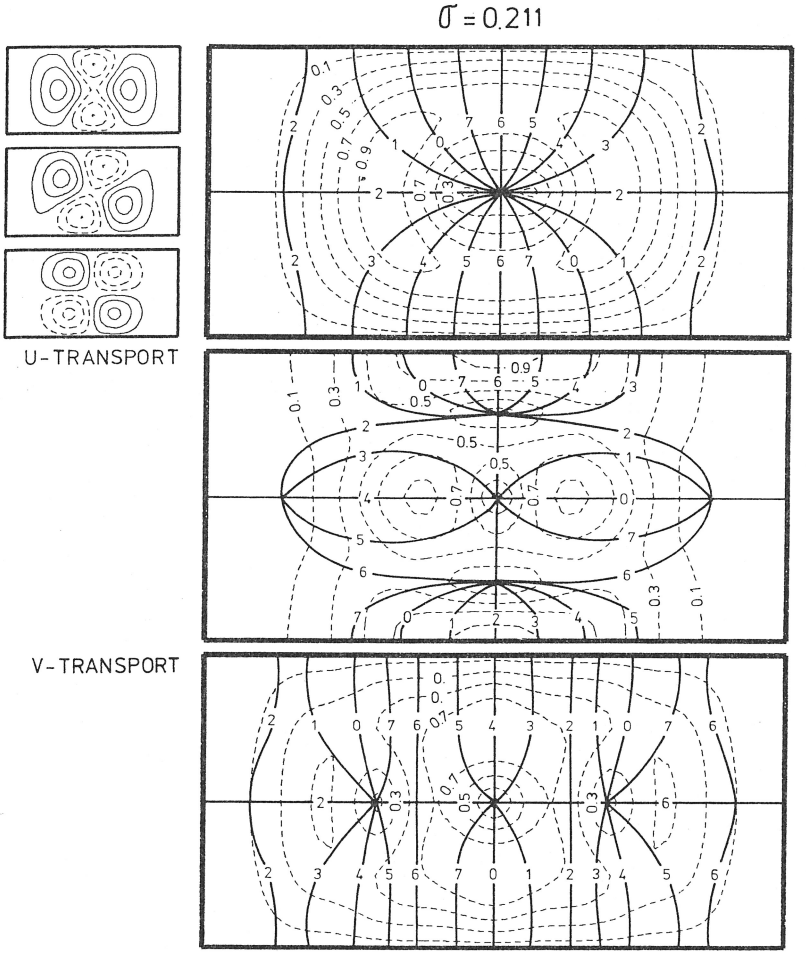

FIGURE 21. Same as Figure 20 for the quadratic Ball-mode.

however, does not lead to resonant bay modes as it only provides a first impression of the possible behavior of the composed geometry. Figure 26 illustrates the configuration in a (x,y)-coordinate system. An infinite trench as an idealized model for a continental shelf of width s communicates with a closed smaller trench of width r and length ℓ; this appended gulf accounts for the estuarine region. The presence of vertical walls at $x = 0$, $y = 0$ and $x = \ell + s$ is a crucial drawback of this model, particularly because topographic waves are studied. It was shown in Stocker and Hutter[1] that presence of discontinuities in the isobaths affects the propagation mechanism of topographic waves considerably. The reason why the trench is used is its analytical simplicity: the dispersion relation $f(\sigma,k) = 0$ is a simple quadratic equation in k and thus, real and complex wave numbers can easily be determined. The latter are known to play a significant role but are cumbersome to calculate for less restrictive geometries.

The trench profiles in the two domains are given by

$$h^e(x,y) = h_0 e^{by}, \qquad 0 \leq y \leq r \tag{20a}$$

for the estuarine channel and

$$h^s(x,y) = h_0 e^{cx}, \qquad \ell \leq x \leq \ell + s \tag{20b}$$

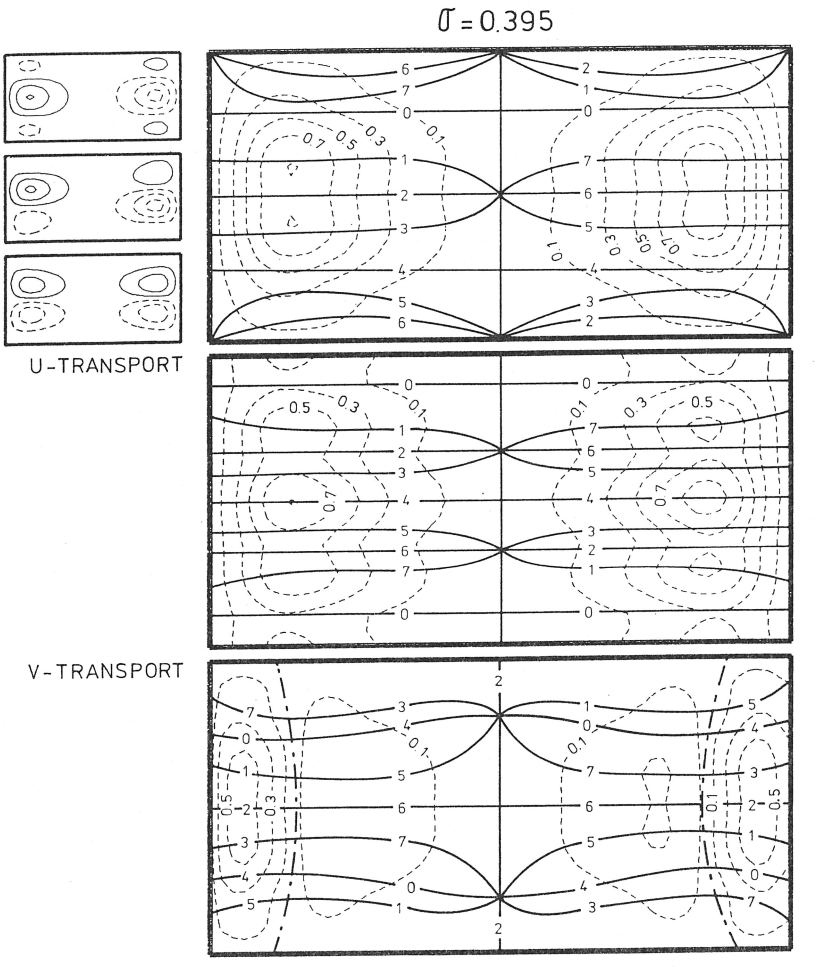

FIGURE 22. Same as Figure 20 for a bay mode. The nodal line (dashed-dotted) is indicated.

for the infinite trench modeling the continental shelf. As demonstrated in Stocker and Hutter[1] the solutions in the respective domains read

$$\psi_n^e = e^{-i\sigma t} e^{(b/2)y} \sin\left(\frac{n\pi y}{r}\right) \exp(ik_n^e x) \tag{21a}$$

$$\psi_m^s = e^{-i\sigma t} e^{(c/2)(x-\ell)} \sin\left(\frac{m\pi(x-\ell)}{s}\right) \exp(ik_m^s y) \tag{21b}$$

and the wave numbers k_n^e and k_m^s of the nth and the mth transverse mode satisfy the dispersion relations.

$$(k_n^e)^2 - \frac{b}{\sigma} k_n^e + \left[\frac{b^2}{4} + \left(\frac{n\pi}{r}\right)^2\right] = 0 \tag{22a}$$

$$(k_m^s)^2 - \frac{c}{\sigma} k_m^s + \left[\frac{c^2}{4} + \left(\frac{m\pi}{s}\right)^2\right] = 0 \tag{22b}$$

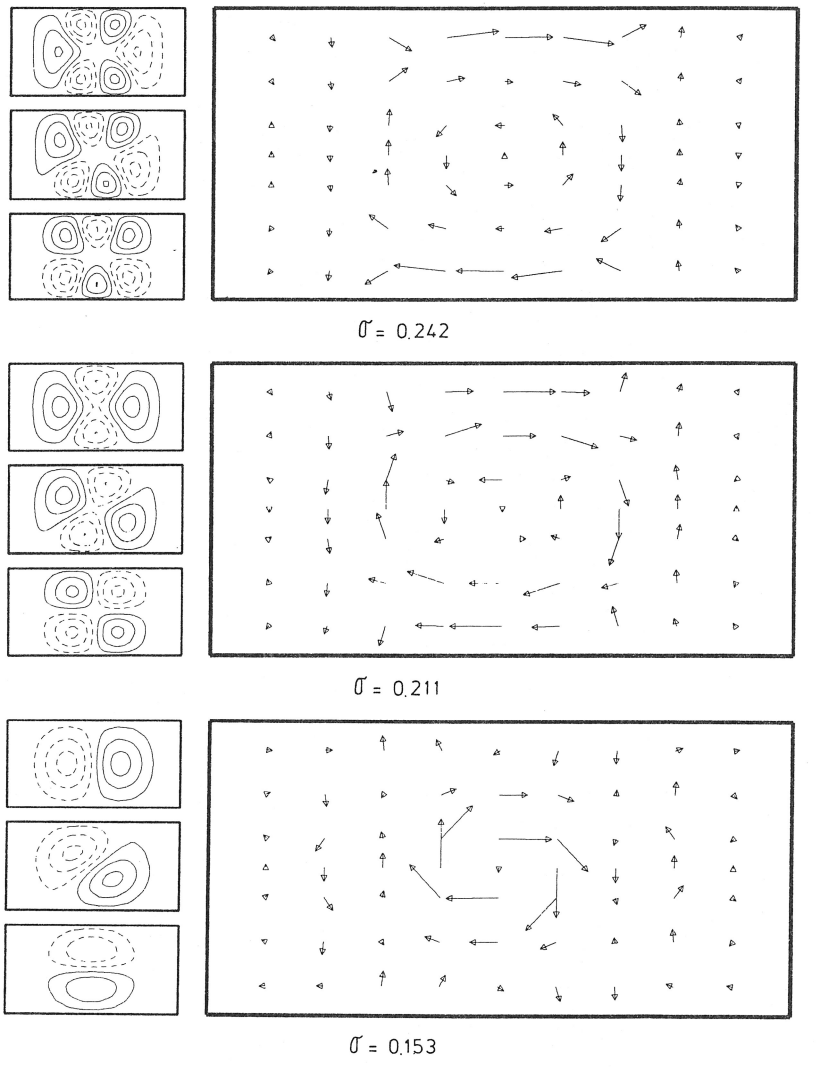

FIGURE 23. Depth-integrated Stokes drift during one period for three Ball-modes.

From these, cutoff frequencies for shelf and estuarine waves can easily be determined. It can be verified that the solutions (Equation 21) satisfy the no flux condition $\psi_n^e = 0$ on the lines $y = 0$, $y = r$, and $\psi_m^s = 0$ on $x = \ell$, $x = \ell + s$. We further require ψ_n^e on $x = 0$ because the estuary is assumed to be closed. In order to achieve no flux across $x = 0$ the stream function ψ_n^e must be a superposition of solutions with the two possible wave numbers k_n^e of the nth mode which satisfy Equation 22a. Equation 21a, therefore, is replaced by

$$\psi_n^e = e^{-i\sigma t} e^{(b/2)y} \sin\left(\frac{n\pi y}{r}\right)[\exp(ik_m^e x) - \exp(ik_{2n}^e x)] \tag{23}$$

describing a standing wave in $0 < x < \ell$. It can be seen that the semi-infinite trench cannot sustain a bay mode which is evanescent away from the wall. We are therefore restricted in this simple model to consider only periodic wave motion (superposed evanescent motion) in the estuary. This implies that the frequency must not exceed the cutoff of the fundamental mode in the estuary, i.e.,

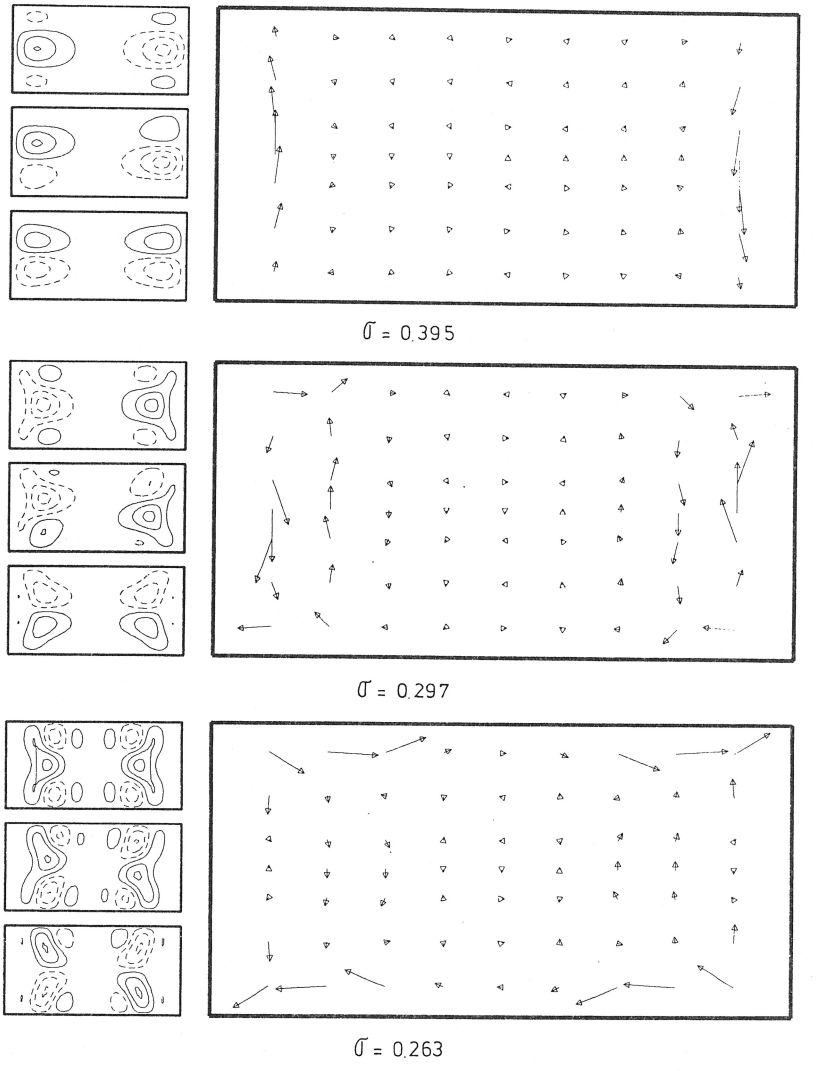

FIGURE 24. Same as Figure 23 for three bay modes.

$$\sigma < \frac{b}{\sqrt{b^2 + (2\pi/r)^2}}$$

The solutions in the respective domains must now be patched together. The junction in the neighborhood of $x = \ell$ has a peculiar structure in that there exists a vertical, roughly triangular wall at $y = r$, $\ell \leq x \leq \ell + br/c$. Γ_2 is its surface projection and Γ_1 is the surface projection of $h^e = h^s$. Aware of the imposed idealizations, we require

$$\left.\begin{aligned} \psi^e &= \psi^s \\ \frac{\partial \psi^e}{\partial y} &= \frac{\partial \psi^s}{\partial y} \end{aligned}\right\} \quad \text{on} \quad \Gamma = \Gamma_1 \cup \Gamma_2 \tag{24}$$

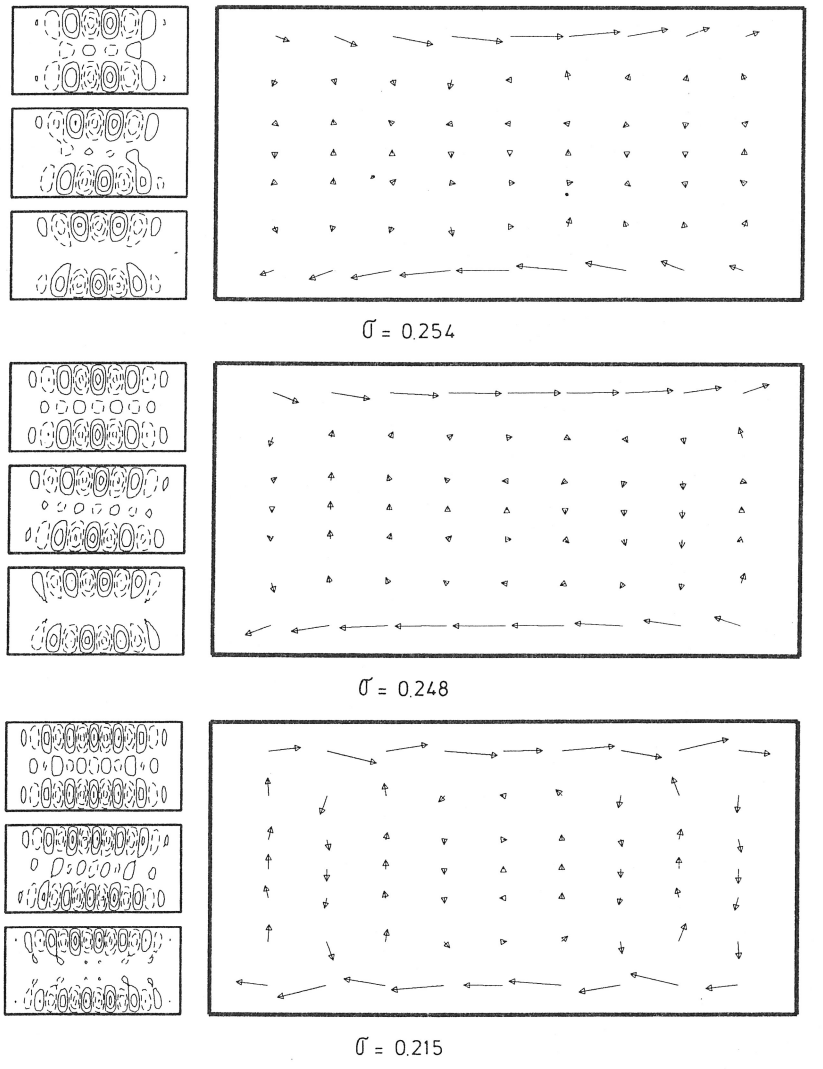

FIGURE 25. Same as Figure 23 for three channel modes.

These statements are reasonable except perhaps for the second one along Γ_2 where the topography is not continuous. The depth of the estuary, however, is much smaller than the shelf depth, i.e., $e^{br} \ll e^{cs}$ and Γ_2 is a very short line. Equally, the jump in h at y = r can be neglected. The continuity of ψ on Γ_2 implies that for ψ^s a superposition similar to Equation 23 must be chosen because ψ^e vanishes on Γ_2. We select for the mth mode

$$\psi^s_m = e^{-i\sigma t}e^{(c/2)x}\sin\left(\frac{m\pi(x-\ell)}{s}\right)\left[\exp(ik^s_{1m}(y-r)) - \exp(ik^s_{2m}(y-r))\right]$$

An exact satisfaction of Equation 24 amounts to the superposition of an infinite number of modes. Let us restrict considerations to one pair (i.e., k^s_{11} and k^s_{21}) of shelf waves of the first transverse mode (i.e., m = 1); trapped shelf modes must not be included. The wave field in the estuary, on the other hand, shall consist of the fundamental pair (Equation 23) with n = 1 and a series n = 2,3,... of evanescent solutions of the form Equation 21a. These are needed to fulfil Equation 24 and are assumed to decay exponentially away from Γ_1 towards x = 0, i.e., $\mathrm{Im}k^e_n < 0$, n = 2,3,... . These preliminaries lead to the solution

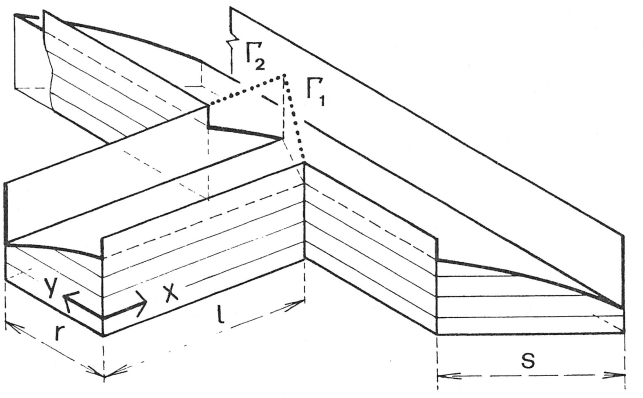

FIGURE 26. Double trench as a crude model of an estuary in connection with a continental shelf.

$$\psi^e = e^{-i\sigma t} e^{by/2}$$

$$\left[E_1 \sin \frac{\pi y}{r} \left[\exp(ik_{11}^e x) - \exp(ik_{21}^e x) \right] + \sum_{n=2}^{N} E_n \sin\left(\frac{n\pi y}{r}\right) \cdot \exp(ik_{1n}^e x) \right] \tag{25}$$

$$\psi^s = S_1 e^{-i\sigma t} e^{cx/2} \sin \frac{\pi(x - \ell)}{s} \left[\exp(ik_{11}^s (y - r)) - \exp(ik_{21}^s (y - r)) \right]$$

which must satisfy Equation 24. The system Equation 25 contains the N + 1 unknown complex coeffieients E_i, (i = 1,..., N) and S_1. These are usually determined by evaluating Equation 24 at M points along the curve Γ. This procedure is called method of collocation or point matching. From Equation 24 follows

$$\psi^e - \psi^s = 0, \qquad \text{on} \qquad \Gamma_1$$

$$\frac{\partial \psi^e}{\partial y} - \frac{\partial \psi^s}{\partial y} = 0, \qquad \text{on} \qquad \Gamma_1$$

$$\frac{\partial \psi^e}{\partial y} - \frac{\partial \psi^s}{\partial y} = 0, \qquad \text{on} \qquad \Gamma_2$$

which at the M points ξ_i, i = 1,..., M on Γ takes the matrix form (assume $E_{N+1} \equiv S_1$)

$$A_{ij} E_j = 0 \tag{26}$$

Therefore, N = 3M − 1 estuarine modes must be superposed and a nontrivial solution can be constructed, provided that

$$\det A_{ij} = 0 \tag{27}$$

This equation selects the distinct frequencies σ at which the shelf wave pattern resonates with the wave motion in the estuary. It is of importance to study the influence of the number of collocation points M (or the truncation order N) on these eigenfrequencies. Table 4 lists a convergence test of the first four eigenfrequencies. Only as few as eight collocation points on Γ yield already a satisfactory value of the eigenfrequency.

TABLE 4
Convergence of Eigenfrequencies Obtained by Equation 27

M	$\ell = 4, r = 1, b = 1, s = 2, c = 1$			
8	0.15284	0.14170	0.12755	0.11338
10	0.15275	0.14143	0.12711	0.11284
12	0.15268	0.14116	0.12680	0.11243
14	0.15261	0.14095	0.12644	0.11197
16	0.15254	0.14082	0.12601	0.11173

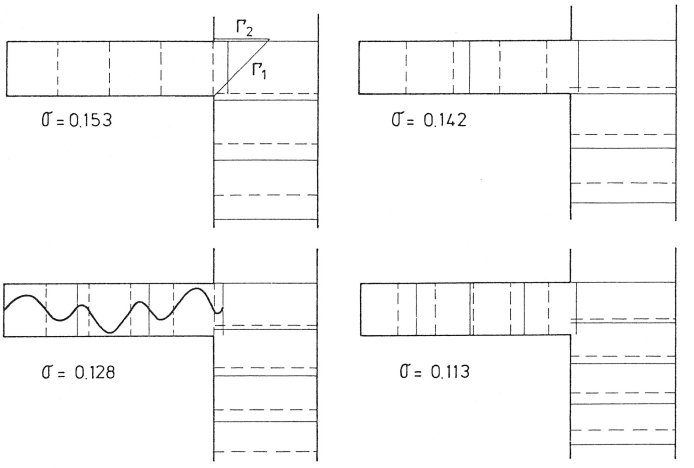

FIGURE 27. Distribution of nodal lines for the first four eigenfrequencies of the double trench shown in Figure 26 having the parameters r = 1, b = 1, s = 2, ℓ = 4, c = 1.

It is instructive to investigate the influence of the five geometry parameters ℓ, r, b, (length, width, and slope of the estuary) and s, c (width and slope of the shelf). For the following, the parameters are selected as follows: M = 8, ℓ = 4, r = 1, b = 1, s = 2, c = 1 unless other values are stated explicitly. Figure 27 shows for the first four lowest eigenmodes how the nodal lines are distributed in the infinite and the finite estuarine trench. In one case we also show the distribution of the stream function. Amplitudes are large between nodal lines with the same signature (dashed-dashed) and small between those having different signature (solid-dashed). With this rule qualitative pictures of the distribution of the stream function can be constructed in the other cases.

Figure 28 shows how the eigenfrequencies of the first nine modes of the double trench vary with the length of the estuarine trench. For each mode σ is monotonically increasing with the length of the estuary and for large ℓ seems to approach the cutoff frequency. Figure 29 shows how the eigenfrequencies of the four first modes vary with the width of the estuary trench (left) and with the strength of the topography, b (right). For all modes, the wider the trench is, the larger the eigenfrequency will be; equivalently, the stronger the trench topography is, the larger the eigenfrequency will become. This effect is particularly pronounced. Finally, in Figure 30 we show the dependence of σ on the width and the topographic strength of the infinite trench. These dependencies are virtually absent or very weak. It follows that the resonating conditions of the double trench are critically influenced by the topographic features of the estuarine trench but only mildly by those of the shelf (which functions as the generator of the resonating effects). This indicates that local resolution of the topography

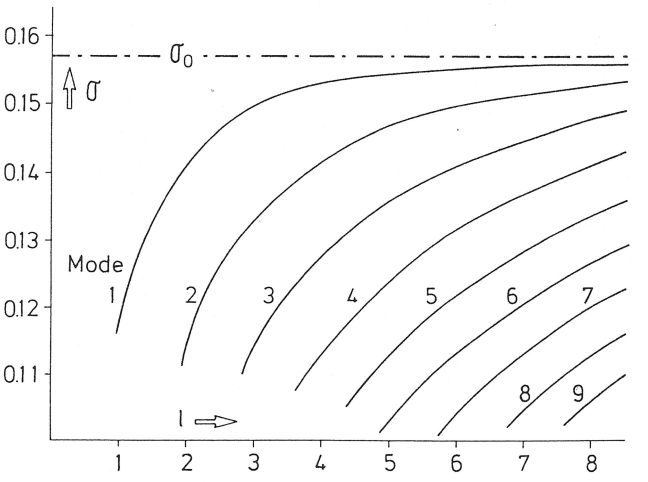

FIGURE 28. The first nine eigenfrequencies of the double trench shown in Figure 26 with parameters r = 1, b = 1, s = 2, c = 1, and $1 < \ell < 8$. Computations were done with M = 8 collocation points. For each mode $\sigma \to \sigma_0$ as $\ell \to \infty$, where σ_0 is the cutoff frequency.

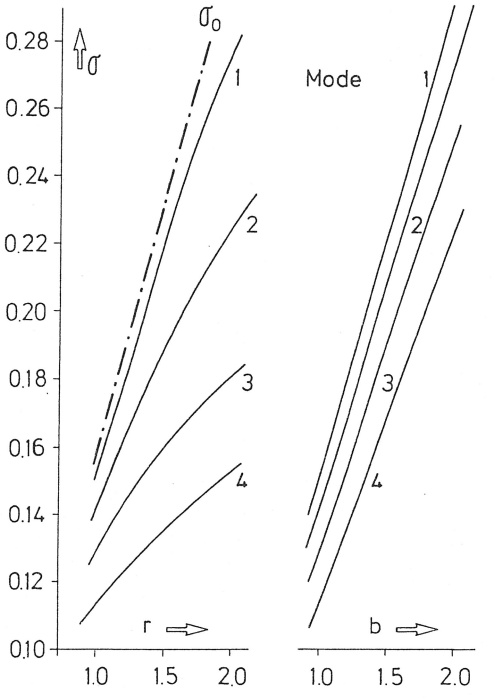

FIGURE 29. The first four eigenfrequencies of the double trench shown in Figure 26 with parameters b = 1 (left) and r = 1 (right); s = 2 and $\ell = 4$. Computations were done with M = 8 collocation points.

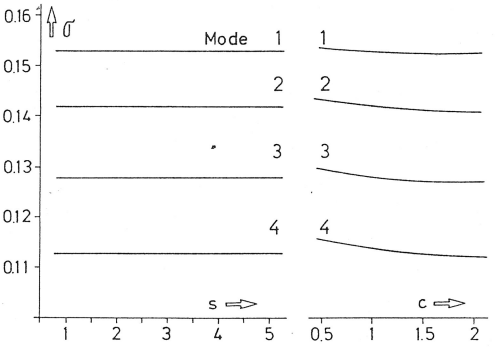

FIGURE 30. Dependence of the first four eigenfrequencies of the double trench shown in Figure 26 on the width s and topography parameter c of the infinite trench. Parameters are c = 1 (left) and s = 2 (right); and r = 1, b = 1, ℓ = 4. The number of collocation points was M = 8.

for topographic waves needs to be accurate, while far field conditions that generate the local activity may well only roughly have to be known.

The recent study by Stocker and Johnson[20] investigates the topographic wave problem in geometries consisting of a shelf channel interrupted by an estuary or a headland.

REFERENCES

1. **Stocker, T. and Hutter, K.,** *Topographic Waves in Channels and Lakes on the f-Plane,* Lecture Notes on Coastal and Estuarine Studies, Vol. 21, Springer-Verlag, New York, 1987.
2. **Johnson, E. R.,** Topographic waves in elliptical basins, *Geophys. Astrophys. Fluid Dyn.*, 37, 279, 1987.
3. **Johnson, E. R.,** A conformal mapping technique for topographic wave problems: semi-infinite channels and elongated basins, *J. Fluid Mech.*, 177, 395, 1987.
4. **Mysak, L. A.,** Elliptical topographic waves, *Geophys. Astrophys. Fluid Dyn.*, 31, 93, 1985.
5. **Buchwald, V. T. and Adams, J. T.,** The propagation of continental shelf waves, *Proc. R. Soc. London Ser. A,* 305, 235, 1968.
6. **Lamb, H.,** *Hydrodynamics,* 6th ed., Cambridge University Press, Cambridge, 1932.
7. **Saylor, J. H., Huang, J. S. K., and Reid, R. O.,** Vortex modes in Southern Lake Michigan, *J. Phys. Oceanogr.*, 10, 1814, 1980.
8. **Ball, T. K.,** Second class motions of a shallow liquid, *J. Fluid Mech.*, 23, 545, 1965.
9. **Mysak, L. A., Salvade, G., Hutter, K., and Scheiwiller, T.,** Topographic waves in an elliptical basin, with applications to the Lake of Lugano, *Philos. Trans. R. Soc. London Ser. A,* 316, 1, 1985.
10. **Mysak, L. A.,** Recent advances in shelf wave dynamics, *Rev. Geophys. Space Phys.*, 18, 211, 1980.
11. **Stocker, T. and Hutter, K.,** One-dimensional models for topographic Rossby waves in elongated basins on the f-plane, *J. Fluid Mech.*, 170, 435, 1986.
12. **Stocker, T. and Hutter, K.,** Topographic waves in rectangular basins, *J. Fluid Mech.*, 185, 107, 1987.
13. **Trösch, J.,** Finite element calculation of topographic waves in lakes, in Proc. 4th Int. Conf. Applied Numerical Modelling, Tainan, Taiwan.
14. **Stocker, T.,** Topographic Waves. Eigenmodes and Reflections in Lakes and Semi-Infinite Channels, Mitteilung No. 93 der Versuchsanstalt fur Wasserbäu, Hydrologie und Glaziologie, ETH Zurich, 1987, 170.
15. **Stocker, T.,** A numerical study of reflections of topographic waves in semi-infinite channels, *J. Phys. Oceanogr.*, 18, 609, 1988.
16. **Ursell, F.,** Mathematical aspects of trapping modes in the theory of surface waves, *J. Fluid Mech.*, 183, 421, 1987.
17. **Stocker, T. and Johnson, E. R.,** Topographic waves in open domains. Part 2. Bay modes and resonances, *J. Fluid Mech.*, 200, 77, 1989.

18. **Gonella, J.,** A rotary-component methods for analysing meteorological and oceanographic vector time series, *Deep-Sea Res.*, 19, 833, 1972.
19. **Huthnance, J. M.,** On trapped waves over a continental shelf, *J. Fluid Mech.*, 69, 689, 1975.
20. **Stocker, T. F. and Johnson, E. R.,** Transmission and reflection of shelf waves by estuaries and headlands, *J. Fluid Mech.*, submitted.